Key Points:
- We adapt a discharge algorithm designed for an upcoming satellite mission for in situ discharge estimation
- The method relies on an array of pressure transducers installed along a mass conserved channel
- Estimating river discharge using multiple pressure transducers is a viable alternative to installing a temporary gauge

Correspondence to:
M. E. Harlan,
mharlan@umass.edu

Discharge Estimation From Dense Arrays of Pressure Transducers

M. E. Harlan[1] , C. J. Gleason[1] , E. H. Altenau[2] , D. Butman[3] , T. Carter[4], V. W. Chu[5], S. W. Cooley[6] , W. D. Dolan[2] , M. T. Durand[7] , E. Eidam[8] , J. V. Fayne[9] , D. Feng[1] , Y. Ishitsuka[1] , C. Kuhn[3] , E. D. Kyzivat[6] , T. Langhorst[2] , J. T. Minear[10] , T. M. Pavelsky[2] , D. L. Peters[11], A. Pietroniro[4,12], L. H. Pitcher[10] , and L. C. Smith[6]

[1]Department of Civil and Environmental Engineering, University of Massachusetts, Amherst, MA, USA, [2]Department of Geological Sciences, University of North Carolina, Chapel Hill, NC, USA, [3]Department of Environmental and Forest Sciences, University of Washington, Seattle, WA, USA, [4]National Hydrology Research Centre, Environment and Climate Change Canada, Saskatoon, SK, Canada, [5]Department of Geography, University of California, Santa Barbara, CA, USA, [6]Department of Earth, Environmental & Planetary Sciences and Institute at Brown for Environment & Society, Brown University, Providence, RI, USA, [7]School of Earth Sciences, The Ohio State University, Columbus, OH, USA, [8]Department of Marine Sciences, University of North Carolina, Chapel Hill, NC, USA, [9]Department of Geography, University of California-Los Angeles, Los Angeles, CA, USA, [10]Cooperative Institute for Research in Environmental Sciences, University of Colorado, Boulder, CO, USA, [11]Watershed Hydrology and Ecology Research Division, Environment and Climate Change Canada, University of Victoria, Victoria, BC, Canada, [12]Department of Civil, Geological, and Environmental Engineering, University of Saskatchewan, Saskatoon, SK, Canada

Abstract In situ river discharge estimation is a critical component of studying rivers. A dominant method for establishing discharge monitoring in situ is a temporary gauge, which uses a rating curve to relate stage to discharge. However, this approach is constrained by cost and the time to develop the stage-discharge rating curve, as rating curves rely on numerous flow measurements at high and low stages. Here, we offer a novel alternative approach to traditional temporary gauges: estimating Discharge via Arrays of Pressure Transducers (DAPT). DAPT uses a Bayesian discharge algorithm developed for the upcoming Surface Water Ocean Topography satellite (SWOT) to estimate in situ discharge from automated water surface elevation measurements. We conducted sensitivity tests over 4,954 model runs on five gauged rivers and conclude that the DAPT method can robustly reproduce discharge with an average Nash-Sutcliffe Efficiency (NSE) of 0.79 and Kling-Gupta Efficiency of 0.78. Further, we find that the DAPT method estimates discharge similarly to an idealized temporary gauge created from the same input data (NSE differences of less than 0.1), and that results improve significantly with accurate priors. Finally, we test the DAPT method in nine poorly gauged rivers in a realistic and complex field setting in the Peace-Athabasca Delta, and show that the DAPT method largely outperforms a temporary gauge in this time and budget constrained setting. We therefore recommend DAPT as an effective tool for in situ discharge estimation in cases where there is not enough time or resources to develop a temporary gauge.

1. Introduction

Historically, hydrologists have relied on water-level gauges to estimate river discharge. By indexing in situ measurements of discharge to the stage at the gauge, continuously recorded stage measurements can be related to discharge through a rating curve, typically to within 4%–12% error compared with an in situ measurement (Horner et al., 2018). When extrapolating for low or high flows, however, these rating curve uncertainties associated with stage-discharge rating curves can increase up to 200% (Kiang et al., 2018). Gauge accuracy comes at a cost: they require substantial human effort to install and maintain and require frequent adjustment via new in situ measurements. Moreover, gauges may become damaged over time from extreme events (e.g., ice jams). In part due to this high maintenance cost, the number of permanent stream gauging stations has decreased since the 1980s across North America (Hannah et al., 2011). Furthermore, for geopolitical reasons, not all gauge data are widely available (Gleason & Hamdan, 2015). Globally, these factors contribute to a depreciated and geographically disproportionate gauge network; only 55% of all countries have contributed river discharge data to the Global Runoff Data Center (GRDC) since 1984

(Fekete et al., 2012). Given these challenges associated with gauges, gauge networks alone are not adequate to assess changes in flow over time at the global scale (Biancamaria et al., 2016).

To account for the dearth of in situ data, hydrologists have turned to remote sensing to estimate discharge. Because discharge cannot be directly measured from space, researchers rely on observable data such as river width, height, surface area, and slope (Alsdorf et al., 2007; Bjerklie et al., 2003, 2005, 2018; Birkinshaw et al., 2014; Brakenridge et al., 2007; Dingman & Bjerklie, 2006; Durand et al., 2014, 2010; Feng et al., 2019; Gleason & Durand, 2020; Gleason & Smith, 2014; Huang et al., 2018; Kouraev et al., 2004; Pavelsky, 2014; Sichangi et al., 2018; Smith, 1997; Smith et al., 1996; Smith & Pavelsky, 2008; Tarpanelli et al., 2015; Van Dijk et al., 2016) or combine remotely sensed data with hydrologic models (Brakenridge et al., 2012; Huang et al., 2020; Nathanson et al., 2012; Neal et al., 2009; Paris et al., 2016; Sun et al., 2018; Yoon et al., 2012). Although these methods have the potential to substantially increase the available discharge record, many still depend on gauges for calibration in some capacity and are limited in temporal resolution (Gleason & Durand, 2020).

NASA's Surface Water Ocean Topography (SWOT) satellite mission (2022 launch) seeks to measure surface water at unprecedented scales using a Ka-band radar interferometer to repeatedly map water surface elevation (WSE) and inundated areas for rivers greater than 100 m wide (Biancamaria et al., 2016). SWOT will measure over 60% of 50,000 km^2 river basins, more than twice the number of basins measured by the GRDC at 30% (Pavelsky et al., 2014). In anticipation of SWOT, several methods have been developed to estimate discharge from its measurements without the use of gauges (Andreadis et al., 2020; Durand et al., 2014; Garambois & Monnier, 2015; Gleason & Smith, 2014; Hagemann et al., 2017; Oubanas et al., 2018). Although SWOT has the potential to vastly improve discharge estimation in ungauged basins, it is primarily designed for large rivers, and it is not expected to provide data on rivers narrower than 50 m wide (Pavelsky et al., 2014). Thus, we must still rely on field techniques to estimate discharge in smaller rivers, tributaries, and headwaters. Therefore, there may be synergies in thinking through these field techniques with a decade of recent remote sensing work in mind.

To measure river discharge in the field, hydrologists principally rely on current meters and hydroacoustic sensors such as an Acoustic Doppler Current Profiler (ADCP) or Acoustic Doppler Velocimeters (ADV; Turnipseed & Sauer, 2010). ADCPs and ADVs are widely used and have substantially reduced in situ measurement time needed to accurately measure discharge. The United States Geological Survey (USGS) and Environment and Climate Change Canada (ECCC) make tens of thousands of streamflow measurements each year, typically to update rating curves at permanent gauging stations, with approximately one measurement per gauge every 5–7 weeks (Turnipseed & Sauer, 2010).

In ungauged rivers, hydrologists use ADCPs and ADVs to provide the discharge measurements needed to create temporary gauges (e.g., Shope et al., 2013). Temporary gauges, typically consisting of a pressure transducer (PT) coupled with a series of discharge measurements, function similarly to permanent gauges but are only deployed for a short time to capture extreme discharge events, avoid seasonal disruptions such as ice formation, or to accommodate budget, time, or geographic constraints. Temporary gauges are commonly deployed by many water agencies and have been studied or used in a myriad of field settings for decades (e.g., Chaudhury et al., 1998; Herbert & Thomas, 1992; Laenen & Hansen, 1985; Miller, 1962; Perry, 2012; Sandberg & Smith, 1995; Wiele & Torizzo, 2003; Ziegeweid et al., 2015). Like permanent gauges, temporary gauges rely on creating a rating curve through pairings of stage and discharge.

Stage variations are measured using a submersible PT fixed at the bottom or side of a river that measures overlying water pressure and is either vented directly to the atmosphere or corrected by an above water barometric pressure sensor. The difference between air and water pressure yields water depth via the hydrostatic equation, which can be converted to WSE through a GNSS survey (Altenau, Moller et al., 2017). PTs are easily deployed, relatively inexpensive, and can be left unattended for months at a time while continuously logging data at a user-defined interval, making them an attractive option for hydrologists. By indexing ADCP discharge measurements to stage or WSE, PTs can be used to create a temporary gauge, yielding discharge at a high temporal resolution for months at a time depending on the site and application. PTs can be telemetered to provide real time monitoring, such as the services provided by the USGS and ECCC, or left in situ until they are physically collected to download data. Obtaining a continuous discharge record at

high temporal resolution (e.g., 15-min resolution), however, is dependent on the ability and time needed to accurately make in situ discharge measurements over a range of flows to adequately build a rating curve. If water levels rise or fall outside of the corresponding measured range of in situ discharge measurements, extrapolation can lead to substantial errors (Coxon et al., 2015; Sörengård & Baldassarre, 2017).

Although temporary gauges represent a common method of field discharge estimation, there are constraints that prevent them from being a viable option for all rivers. Obtaining discharge measurements at low and high flows is needed to develop a robust rating curve. This often necessitates multiple revisits over weeks or months depending on the variability of the annual flow regime. For example, an arid catchment with a spring snowmelt pulse would require visits in the spring high flow and autumn low flow periods. The use of ADCPs or ADVs may also require a nearby bridge, hydroboard, tag line, or boat which may not be conducive to all field settings. These considerations elongate the time and cost required to create an accurate stage-discharge rating curve for a temporary gauge. Although temporary gauges present a potentially accurate means to measure discharge to supplement permanent hydrometric networks, the time needed to fully develop the rating curve, the cost and expertize needed to operate them, and the inherent limitations of the instruments impede this method from being more broadly applied.

As a means to overcome the limitations associated with temporary discharge gauges, we introduce a novel method of field discharge estimation that can be robustly applied to any river location with in situ access. The only in situ data needed for this method are arrays of PTs, and hence, we refer to this method as the Discharge via Arrays of Pressure Transducers method, or DAPT. We combine PT data with globally available digital elevation models (DEMs) and a discharge algorithm developed for remote sensing to provide streamflow estimates. Here, we describe DAPT and address the following three questions: (Q1) *How robust is DAPT to changes in input data and model parameters?*; (Q2) *How does DAPT compare to a temporary gauge?*; and (Q3) *How well can DAPT reproduce in situ discharge measurements in a realistic field setting?*

To answer Q1, we explicitly validate our method in gauged rivers and test its sensitivity to all physical and algorithmic parameters. For Q2, we compare DAPT to temporary gauges built from the same PT and discharge data within the same gauged rivers used for Q1. Lastly, for Q3, we present a case study of this method in a remote setting over two years of fieldwork in a poorly gauged site: only 4 of 11 demonstration river reaches have hydrologically relevant permanent gauge information. We find that DAPT is robust when discharge is well constrained and can perform similarly to a temporary gauge, and recommend it as an effective means to estimate discharge without needing to fully develop a rating curve.

2. Experimental Setup

2.1. Experimental Design

To answer our science questions, we designed a series of sensitivity tests followed by a case study (Figure 1). To address Q1 and Q2 we installed dense arrays of PTs on five permanently gauged rivers during open-water periods spanning 2014 to 2017 in the context of SWOT cal/val development, hereafter referred to as the TOWNS data set (Tanana, Olentangy, Willamette, North Saskatchewan, Sacramento, described in detail in Section 2.2). DAPT combines the PT data with globally available DEMs and a recent SWOT discharge algorithm, Bayesian-AMHG-Manning (BAM, Section 2.3), to estimate discharge. To collect data for our case study and address Q3, we deployed PT arrays (2018–2019) in nine rivers in a remote deltaic setting (the Peace-Athabasca Delta or PAD, Canada). We collected extensive in situ ADCP discharge measurements for validation in these ungauged rivers. Further details for the sensitivity tests and case study are described below.

2.1.1. Q1: How Robust is DAPT to Changes in Input Data and Model Parameters?

To examine the robustness of DAPT using the TOWNS data set, we evaluated the method across five sensitivity tests split into two categories: PT sensitivity and BAM sensitivity (Figure 1). For each test we varied $_nC_k$ combinations of the chosen sensitivity, where n is the total possible inputs to the test and k represents the number of inputs that vary. To reduce the number of overall model runs, we randomly sampled 10 combinations if $_nC_k$ was greater than 10. In the first three tests, we varied the number of PTs (Test 1), spacing between PTs (Test 2), and temporal resolution of PTs (Test 3). In some cases, PTs were installed strategically
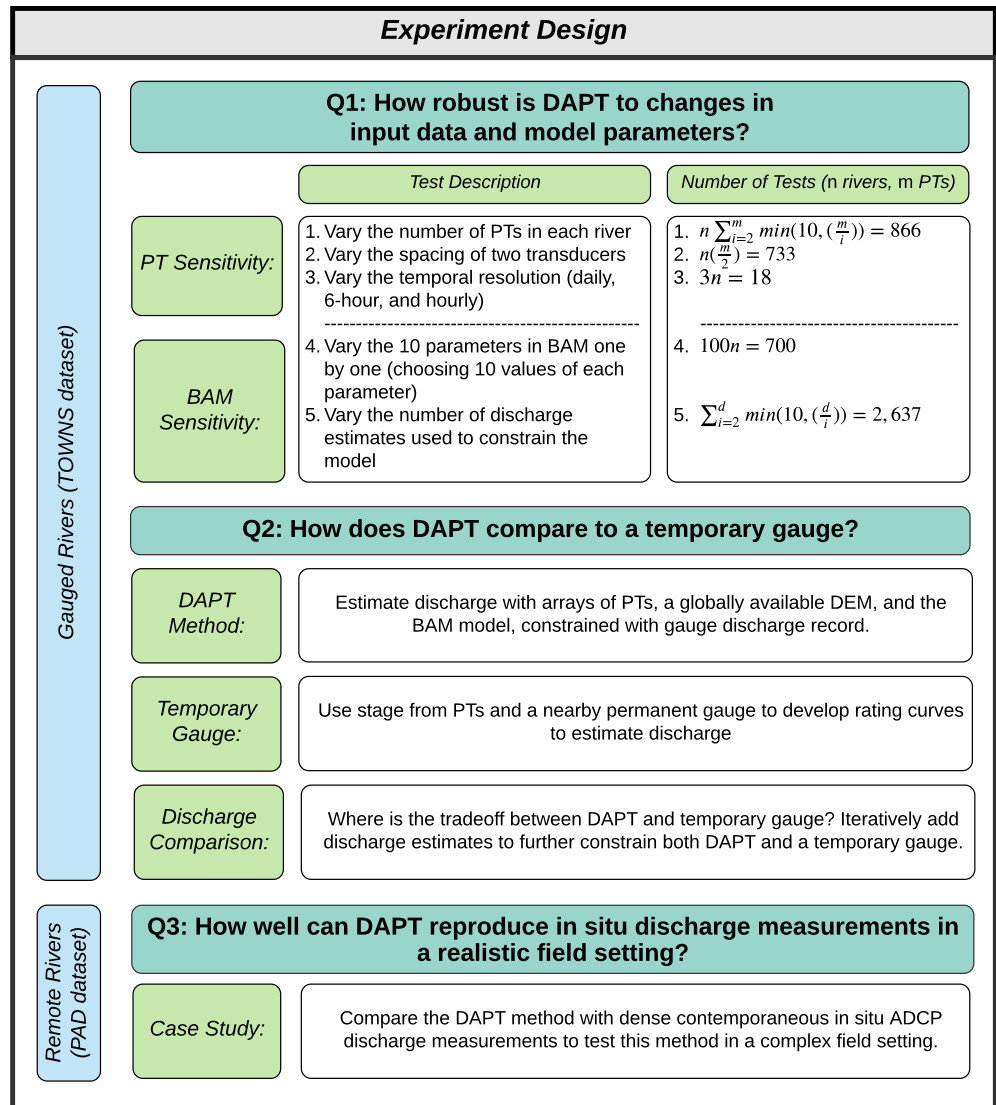
Figure 1. Our experiment design treats the first two science questions as sensitivity tests in gauged rivers, and the third question as a case study in a remote setting. We run five different sensitivity tests for Q1, with the corresponding number of model runs displayed on the right. Q2 compares the added benefit of discharge measurements to both DAPT and the standard approach of a temporary gauge. Lastly, we compare the DAPT method with in situ discharge measurements in poorly gauged rivers to answer Q3. DAPT, discharge via arrays of pressure transducers.

to capture hydraulic features, and thus we iterated over all PTs to account for the nonrandom installation in Test 2.

For the BAM sensitivity in Test 4 we used a stationary permanent gauge installed by either USGS or ECCC to calibrate each BAM parameter, and then artificially degraded parameters to examine model robustness. We used a leave-one-out construction to hold all model parameters except one at their true value. To sample a range of parameter values, we used distributions based on the input data described in Section 3. In Test 5, we iteratively added one gauge-derived discharge estimate at a time to the discharge prior (Q_{prior}) to ascertain the added benefit of each additional discharge estimate, and refer to this sensitivity as numQ_{prior}.

2.1.2. Q2: How Does DAPT Compare to a Temporary Gauge?

To address Q2, we compared discharge estimates from DAPT to the discharge estimated from a temporary gauge created by pairing our PTs with a timeseries of discharge from a nearby permanent gauge for rivers in the TOWNS data set. Thus, for every PT we installed, we made a unique rating curve, and this PT and rating

curve together define a "temporary gauge." Since DAPT inherently relies on multiple PTs, we compared the ensemble of rating curve discharge estimates to DAPT for a fairer comparison. We repeated the discharge sensitivity test (Test 5) to understand the sensitivity of both DAPT and the temporary gauge ensemble to the size and variability of Q_{prior}.

We note here that we rely on discharge from a permanent gauge rather than ADCP or ADV measurements to train and test our methods. By definition, this gauged discharge has a strong correlation with our WSE measurements, thus this comparison favors a temporary gauge in the gauged set of rivers. An alternative approach would use archived discharge measurements to develop rating curves, but there were not sufficient archival USGS or ECCC discharge measurements at similar water levels to our PT installations for a meaningful comparison, with a maximum of 10 measurements per river reach over a 10-year period reported in the USGS/ECCC archives.

2.1.3. Q3: How Well Can DAPT Reproduce In Situ Discharge Measurements in a Realistic Field Setting?

Following these sensitivity tests, we present a case study in a poorly gauged set of rivers in the Peace-Athabasca Delta (PAD) to answer Q3. This setting (Section 2.2) is ideally suited to DAPT given its complexity, remoteness, size, and number of channels in close proximity. Although the PAD is gauged for flows entering and exiting the delta, water level stations within the connected channel-lake system operated by ECCC do not commonly provide discharge. We made discharge measurements with an ADCP for validation and to constrain the DAPT parameters in conjunction with sensitivity results learned from the TOWNS tests. We again compare DAPT with a temporary gauge, repeating Q2 sensitivity tests for DAPT and a temporary gauge using the same PT and ADCP data. There are no gauges used to train either DAPT or temporary gauges in the PAD, and unlike the TOWNS data set, we assumed no other prior knowledge of discharge in the PAD.

2.2. Study Areas

In total, we tested DAPT on 18 reaches of 14 different rivers using dense arrays of PTs, installed from 2013 to 2019. We utilized data from two different settings: a five-river data set where temporary PT arrays were installed near USGS and ECCC gauges (TOWNS), and a nine-river field experiment in a remote sub-Arctic environment (PAD) without permanent discharge gauges. The TOWNS data include the following rivers: Tanana (AK), Olentangy (OH), Willamette (OR), North Saskatchewan (Canada), and the Sacramento (CA) (Figure 2). These rivers allow us to test the sensitivity of the method with full knowledge of discharge. In total, we completed 4,954 model runs across all five rivers at a daily resolution, a number that represents the sum of the tests outlined in Figure 1. Following these sensitivities, we explicitly compare DAPT with a temporary gauge using discharge derived from a permanent gauge (Q2).

We used the PAD rivers as a case study to validate DAPT in a remote, poorly gauged discharge environment. The PAD is North America's largest inland delta characterized as a hydrodynamic floodplain area sensitive to climate variability and development in upstream areas (e.g., hydroelectric dams and mining). Thus, changes in inflows and wetland-lake storage are simultaneously vital and difficult to monitor (Peters et al., 2006; Prowse & Conly, 2000; Toth et al., 2006).

Table 1 displays the mean discharge, mean width, strength of the rating curve, sampling period, number of loggers, temporal resolution, the closest USGS or ECCC gauging station, number of validation discharge measurements, and DEM and DEM resolution for all sites. The Sacramento River was split into three reaches to account for differences in PT installation time. In the PAD, the Athabasca and Rochers rivers were split into two separate reaches to account for the presence of tributaries. Here we explicitly define the length of our river reach as the distance between the first and last PT.
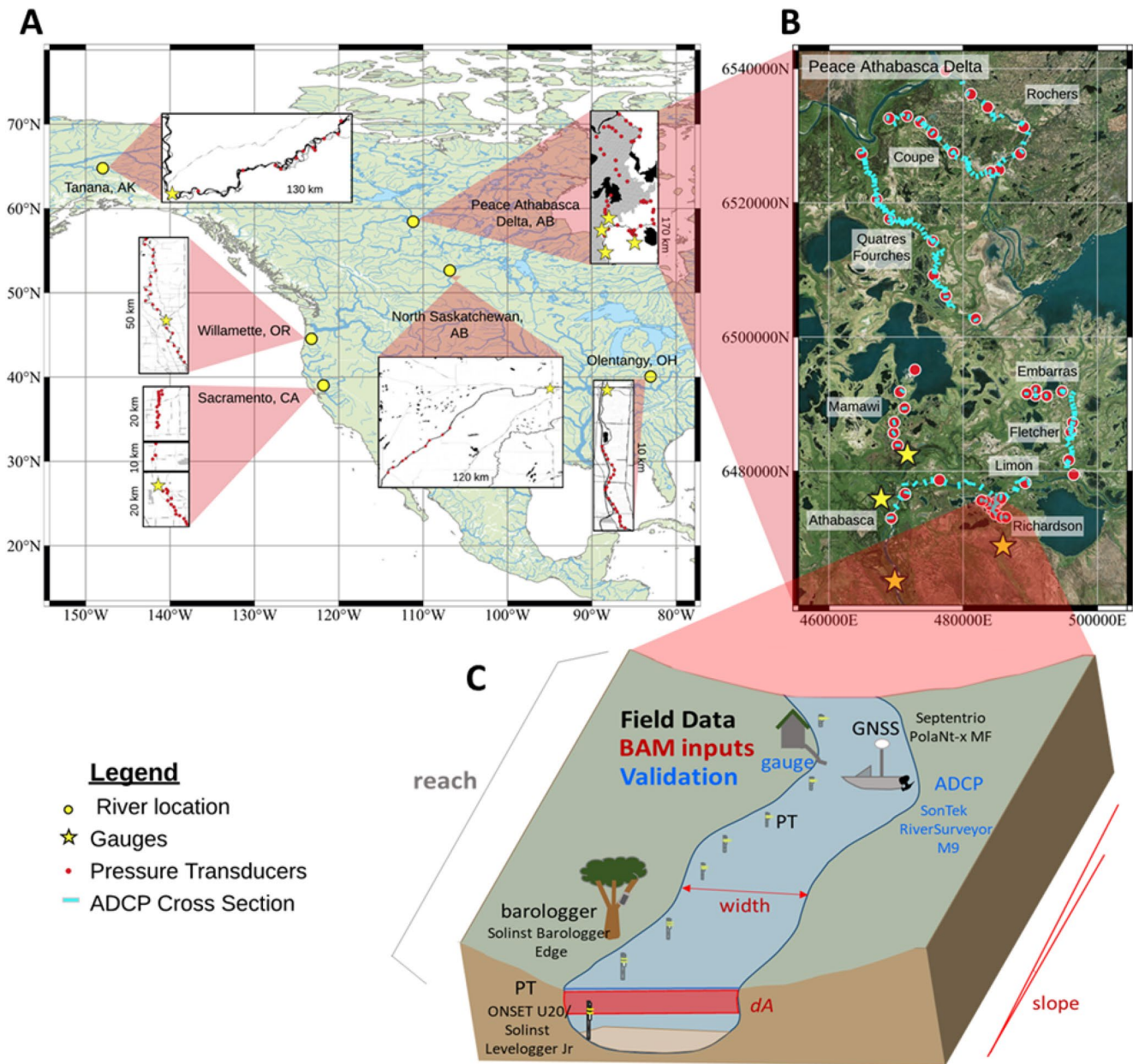
Figure 2. Panel A displays both the TOWNS and PAD locations. The PAD is displayed in further detail in Panel (b) Nearby USGS and ECCC gauge stations are shown as yellow stars, while ADCP discharge measurement locations are shown in cyan lines and PT locations as red circles. Each site is scaled differently, with lengths shown on the side of each cutout. Panel C displays a visual schematic of data sources (black), BAM inputs (red), and validation data (blue). PTs are installed in the riverbed (shown in gray). Barologgers are either attached to trees along the shore (as pictured), or rebar on the riverbank. Discharge validation comes from either a gauging station (TOWNS), or boat-based ADCP measurements (PAD). ADCP, acoustic doppler current profiler; ECCC, Environment and Climate Change Canada; PAD, Peace-Athabasca Delta; USGS, United States geological survey.

2.3. Data

2.3.1. Water Surface Elevation

Each of our 14 sites contains arrays of 5–35 PTs spaced between 100 m and 25 km apart depending on the river. In the Tanana river, Solinst Levelogger Jr PTs were deployed in the river bed secured to either cinder blocks or dumbbells and used nearby barologgers for atmospheric pressure corrections (Altenau, Moller et al., 2017). Stage measurements were converted to WSE using an optical auto-level survey to measure the height difference between the water surface and GNSS surveyed benchmarks. These GNSS measurements

Table 1
Study Area Description

River	Mean discharge (m³/s)	Mean width (m)	Rating curve corr. coef. *r*	Dates (MM/DD/YY)	PT count	Rec. Int. (min)	Nearby gauge ID	Discharge count	DEM	DEM res. (m)
Tanana	691	653	0.99	5/20/15–6/19/15	12	2	15515500	3,056	ArcticDEM	2
Olentangy	3	48	0.89	12/4/14–12/17/14	20	15	03226800	925	NED	10
Willamette	198	139	0.59	3/14/15–5/3/15	21	14	14166000	4,988	NED	10
N. Saskatchewan	306	309	0.86	6/28/17–8/10/17	9	5	05GG001	42	CDEM	30
Sacramento R1	147	136	0.99	3/5/15–3/18/15	10	15	11389500	1,232	NED	10
Sacramento R2	122	92	0.93	3/17/15–5/12/15	6	15	11389500	5,349	NED	10
Sacramento R3	128	199	0.88	3/23/15–5/27/15	19	15	11389500	6,678	NED	10
Athabasca R1	841	225	0.27	8/7/18–10/1/18	2	5	07DD001	4	CDEM	30
Athabasca R2	876	225	0.48	8/7/18–10/1/18	3	5	07DD001	42	CDEM	30
Coupe	91	93	−0.27	8/8/18–9/29/18	5	5	–	63	CDEM	30
Embarras	140	77	0.47	7/12/19–8/18/19	2	15	–	12	CDEM	30
Fletcher	153	85	0.09	8/7/18–9/30/18	3	5	–	52	CDEM	30
Limon	39	36	0.32	7/13/19–8/18/19	4	15	–	9	CDEM	30
Mamawi	110	61	−0.04	8/7/18–9/30/18	4	5	07KF015	20	CDEM	30
Quatre Fourches	346	111	−0.60	8/6/18–9/30/18	6	5	–	158	CDEM	30
Richardson	15	39	0.40	7/13/19–8/18/19	5	15	07DD002	26	CDEM	30
Rochers R1	1,890	277	−0.24	8/6/18–9/30/18	2	5	–	18	CDEM	30
Rochers R2	1,649	277	0.12	8/6/18–9/30/18	3	5	–	27	CDEM	30

Notes: Mean discharge and mean (river) width represent the mean values over the time period of this study (shown in the dates column). Rating curve correlation coefficient *r* corresponds to the correlation between logged WSE and discharge for each of the rivers, highlighting the relatively weak correlation in the PAD data set compared to the TOWNS data set. PT count refers to the number of pressure transducers in each reach and Rec. Int. refers to measurement frequency (minutes). Discharge count gives the number of permanent gauge (TOWNS) or ADCP (PAD) discharges available for training/validation. DEM refers to the digital elevation model used to estimate river width and slope further described in Section 3.4, with the corresponding resolutions to the right. ADCP, acoustic doppler current profiler; CDEM, Canadian digital elevation model; DEM, digital elevation models; NED, National Elevation Dataset; PAD, Peace-Athabasca Delta; WSE, water surface elevation.

were processed using Natural Resources Canada's Canadian Geodetic Survey Precise Point Positioning (PPP) tool. For the Olentangy, the same Solinst Levelogger Jr PTs were deployed attached via cinder blocks near barologgers, and a Leica Viva GS15 RTK GPS rover was used to convert stage to WSE (Tuozzolo, Lind et al., 2019). In the North Saskatchewan, Willamette, and three Sacramento reaches, ONSET U20 PTs were deployed alongside barologgers within open-ended PVC tubes for protection, and similarly surveyed in with RTK GPS (Minear & Wright, 2016; Tuozzolo, Langhorst et al., 2019). To stabilize the PTs in place, a 1 m long by 0.012 m diameter rebar metal stake was driven into the riverbed, leaving 0.20 m above to attach the PT with plastic zip ties. A visualization of the installation is outlined in Figure 2. This particular PT setup differs from a standard gauge in that real-time monitoring is not available, as providing telemetry for PTs is prohibitively expensive while decreasing physical robustness. Instead, data were downloaded at the end of the field campaign upon PT removal.

In the PAD, we deployed transducers in two separate field seasons. We deployed 44 Solinst Levelogger Junior Edge PTs in 2018 attached via cinder blocks and coupled these with a total of 352 ADCP discharge measurements collected across six larger rivers. In 2019, the field team returned to focus on smaller tributaries: deploying 20 transducers and collecting 83 ADCP discharge measurements across three more rivers. Barometric transducers were installed every 10 km via zip ties within a tree, roughly 2 m above the water surface. Each approximate transducer location was identified with a Garmin eTrex 20x GPS, and the WSE was determined through mooring a boat over the transducer for two minutes and measuring the offset from the boat-based GNSS unit to the water level. GNSS measurements were made with a Septentrio PolaRX5 receiver logging at 1 Hz with a Septentrio PolaNt-x MF antenna mounted on a 2 m pole mounted to the

back of the boat and processed with CSRS PPP. Expected error associated with the WSE profiles for each of the rivers combines uncertainty from GPS surveys, PTs, and barologgers, and is estimated at 10 cm or less.

2.3.2. Discharge Validation Data

In the TOWNS data set, we relied on permanent gauging stations maintained by either the USGS or ECCC for discharge validation. Each of these stations was within 50 km of the nearest PT and contained discharge data at 15-min intervals for the time period the PTs were deployed (Table 1). We assumed that the river reaches are mass-conserved based on the similarity in PT data and distance between transducers, and thus have the same discharge throughout our reaches. We are aware that in the Tanana and Olentangy rivers ungauged tributaries impact this assumption, but previous investigation on these reaches has asserted that these tributaries contribute an estimated maximum mass imbalance of 14% (Altenau, Bates et al., 2017; Tuozzolo, Lind et al., 2019; Tuozzolo, Langhorst et al., 2019).

In the PAD, we relied on SonTek RiverSurveyor M9 ADCP discharge measurements for validation in most cases, as there are very few gauges available. The instrument was mounted to the side of a motorboat and used to estimate discharge via two orthogonal transects at a given location throughout the river reaches surveyed in the PAD. We processed the data using SonTek's RiverSurveyorLive software, and only included measurements that met the following criteria: (1) total discharge between right and left transects agreed within 5%, (2) at least 70% of the wetted width was measured by the ADCP, (3) the ratio of average boat speed to average water speed was less than 1.5, (4) the battery voltage of the ADCP was sufficiently high (at least 12 V), (5) measurements made at the river edge were sufficiently dense (have at least 10 edge samples that have at least 2 cells of depth), (6) the track and depth reference were high quality (all samples in the transect have a track reference code in SonTek's system), (7) river velocity vectors appear perpendicular to boat motion, do not cross each other, and do not move upstream, (8) the ADCP beams were working correctly (i.e., there were no beam separation errors), and (9) the channel width, channel area, and average velocity are consistent with other profiles at the same location and same time, where applicable. Discharge measurements were made within 2 km of transducer locations, and along the reach where possible over the course of several days.

In total, we made 352 ADCP discharge measurements over 11 reaches while traveling over 2,000 river km in the PAD. Despite this large effort, this is not a traditional discharge monitoring effort for the purposes of establishing a temporary gauge. This study prioritized rapidly deploying pressure transducers over a large area instead of spending time collecting repeated ADCP data at a few locations. For instance, we made dozens of ADCP measurements in a single day or over two days for most reaches, thus capturing very little flow variability. We aimed to estimate discharge from PTs without having to fully develop rating curves, and thus wanted to test the effectiveness of relying on dense PT data with only a few ADCP measurements as input for BAM. Therefore, we constrain our primary temporary gauge/DAPT comparison to the TOWNS data set where our in situ measurements span a wider range of days and flow levels. We do, however, provide the corresponding temporary gauge performance in the PAD.

2.3.3. Digital Elevation Models

This study used different digital elevation models (DEMs) depending on availability. In the Olentangy, Sacramento, and Willamette, we used the USGS 3D Elevation Program at ⅓ arc second (~10 m) resolution referenced in the North American Vertical Datum of 1988 (NAVD88) and published in 2013 (https://www.usgs.gov/core-science-systems/ngp/3dep). In the Tanana, as it is within the Arctic circle, we relied on Arctic DEM at a 2 m resolution referenced to the WG84 ellipsoid and updated in September 2018 (Porter et al., 2018). Lastly, in the North Saskatchewan and PAD, we used the Canadian Digital Elevation model (CDEM) at 30 m resolution, updated in 2011 (https://open.canada.ca/data/en/dataset/7f245e4d-76c2-4caa-951a-45d1d2051333), and referenced in the Canadian Geodetic Vertical Datum of 1928 (CGVD28). These DEMs were used to estimate river width (TOWNS) and slope (Sections 4.2.1 and 4.2.2) alongside manually digitized river centerlines. Although higher resolution Lidar DEMs exist for several of these rivers, we relied here on regionally available DEMs to provide results from standardized and widely available inputs and provide a sense of the adaptability of this method in different environments.

3. Methods

3.1. Discharge Algorithm for the TOWNS Tests

To estimate discharge from these unique datasets we used the Bayesian-AMHG-Manning (BAM) algorithm (Hagemann et al., 2017). BAM estimates discharge given anticipated SWOT river measurements of width, height, and slope, and is one of several SWOT-related discharge algorithms (Andreadis et al., 2020; Durand et al., 2014; Garambois & Monnier, 2015; Gleason & Smith, 2014; Oubanas et al., 2018). Specifically, BAM is a Mass conserved Flow Law Inversion algorithm (Gleason et al., 2017). BAM uses two different flow laws to estimate discharge: AMHG (Gleason & Smith, 2014), which relies on width only, and Manning's equation, which relies on river width, slope, and cross-sectional area. In this study, we make use of the multitude of inputs available from the PT data. River widths are estimated through a coarse DEM and are not sensitive to small changes in WSE (Section 3.2), so using the less width-dependent Manning's equation allows for more variation in input data compared to AMHG. At a multi-reach scale, Manning's equation is presented in Equation 1 following Durand et al. (2014), where i and t represent cross sections and time, respectively, Q is the discharge (m^3/s), n is the Manning roughness coefficient, A_0 is the unobserved cross-sectional area (m^2), dA is the observed change in cross sectional area (m^2), W is the width (m), and S is the slope (m/m):

$$Q_t = \frac{1}{n}\left(A_0 + dA\right)_{it}^{5/3} W_{it}^{-2/3} S_{it}^{1/2} \tag{1}$$

3.2. Discharge Algorithm Inputs

To estimate discharge, BAM requires measurements of widths, slopes, partial flow areas, and "prior" estimates of unobserved quantities. These Bayesian "priors" are probability distributions that specify the a priori uncertainty about unknown parameters described in Section 4.2.4. The rest of this section describes how we derived BAM inputs from our field PT installations, visualized in Figure 2.

3.2.1. Width

Width is easily estimated from remote sensing, and previous studies have relied on satellite imagery (e.g., Feng et al., 2019), topography photogrammetrically extracted from high-resolution aerial imagery (King et al., 2018), datasets such as Global River Widths from Landsat (GRWL; Allen & Pavelsky, 2018), or DEMs such as MERIT Hydro (Yamazaki et al., 2019). However, these methods require continuous remote sensing to estimate width at the time of a PT record, which was not available for this study. Here we estimated width by generating a cross sectional elevation profile from a DEM orthogonal to a manually digitized centerline of the reach. Elevations at the water surface for these DEMs are smoothed, making them visually distinguishable from surrounding land. At each PT location, we manually identified the left and right banks, linearly interpolated a smooth slope for each to eliminate the "steps" in the DEM, and intersected the WSE with these smooth banks to estimate width.

For the Olentangy, we were able to validate these width estimates with widths from a rangefinder and found the estimates to be comparable (within ± 5 m on average; Tuozzolo, Lind et al., 2019). For the remaining TOWNS data set, we validated our width estimates with the GRWL data set and found general agreement with an average discrepancy of 22%. This width estimation method works well for when the water surface is close to or above the water surface of the DEM, however, when PTs record WSE below the DEM, we must rely on extrapolation. To extrapolate width from a DEM, several nonlinear methods have been suggested and successfully employed (Mersel et al., 2013; Schaperow et al., 2019), but here we rely on linear interpolation given the coarseness of the DEM resolutions: these sophisticated methods are inappropriate given our relatively small amount of data.

3.2.2. Slope

To estimate river slope, we calculated water surface slope at each PT location by differential leveling of sequential PTs. We used this particular method of obtaining slope to capture temporal variations in slope over time, as opposed to assuming a constant slope through measuring the instantaneous slope given by the DEM, which is temporally invariant and may not be accurate to the river conditions for this study period.

Table 2
BAM Prior Descriptions

Prior description	Symbol	Minimum	True	Maximum	Related priors
Discharge (Q)	Q_{prior}	min(Q_{obs})	Q_{obs}	max(Q_{obs})	$\log \widehat{A_0}$
	$\log Q$	$\log[\bar{Q}_{obs} - 4\sigma_{Qobs}]$	$\log[\text{median}(Q_{obs})]$	$\log[\bar{Q}_{obs} + 4\sigma_{Qobs}]$	
	$\log \sigma_Q$	$0.1\log[\sigma_{Qobs}]$	$\log[\sigma_{Qobs}]$	$10\log[\sigma_{Qobs}]$	
Manning's n (n)	$\log \hat{n}$	$\log(0.02)$	$\log(0.035)$	$\log(0.15)$	$\log \widehat{A_0}$
	$\log \sigma_n$	0.028	1.413	2.80	$\log \sigma_{A0}$
Invariant area (A_0)	$\log \widehat{A_0}$	$[\min(n) \times \min(Q_{obs}) \times \min(W_{obs})^{2/3} \times \max(S_{obs})^{-1/2}]^{3/5}$	$(0.035 \times \bar{Q}_{obs} \times \bar{W}_{obs}^{2/3} \times S_{obs}^{-1/2})^{3/5}$	$[\max(n) \times \max(Q_{obs}) \times \max(W_{obs})^{2/3} \times \min(S_{obs})^{-1/2}]^{3/5}$	$\log \hat{Q}$ $\log \hat{n}$
	$\log \sigma_{A0}$	$0.1\log \sigma_{dAobs}$	$\log \sigma_{dAobs}$	$10\log \sigma_{dAobs}$	
Input errors	σ_{Serr} [m/m]	$0.01*\bar{S}_{obs}$	$0.1*\bar{S}_{obs}$	$\bar{S}_{obs}$	
	σ_{dAerr} [m^2]	3	30	300	
	σ_{Werr} [m]	3	30	300	
Bounds	bounds	Mean(prior) +/− 0.1σ	Observed bounds	Mean(prior) +/− 3σ	$\log Q$ A_0 $\log \hat{n}$

Notes: Discharge, Manning's n, invariant area, and width are all truncated priors, with upper and lower bounds and sample means and standard deviations given by ˆ and σ. Each of these priors can vary within the specified distributions, which are further truncated based on the "bounds" parameter. In total, we directly varied these 11 parameters for each river, which were used to set 15 of 28 total BAM priors. The remaining 13 priors are left at the default BAM value, as they are not directly related to river characteristics or influenced by PTs.

3.2.3. Partial Area

Partial area, referred to here as dA, is defined as the change in the cross-sectional area with respect to time. A_0 can be conceptualized as the median cross-sectional area typically observed at minimum flows and is treated as a prior instead of direct input, as we do not have bathymetric data on each river. Separating the area into dA and A_0 in Equation 1 allows for an estimate of area without bathymetric or low-flow observations. In this case, we calculated dA as the Riemann sum approximation of the integral of width times the change in river height.

3.2.4. Priors

BAM uses several priors to specify the a priori uncertainty in unobserved parameters. The term "prior" is inherited from Bayesian statistics. Essentially, any knowledge we had previously about any relevant parameter from any source is a "prior," where Bayesian priors are defined as a mean value and uncertainty. Priors include discharge (Q_{prior}), Manning's roughness coefficient n, and the median low flow area for each cross section (A_0). BAM has default values for each of these parameters based on the hydroSWOT database (Canova et al., 2016). Both DAPT and a temporary gauge require a discharge prior, which can come from field data (as in this study) or modeled estimates. Therefore, in situ discharge from an ADCP, discharge from a previous gauge, or discharge from a model could all be considered priors. For a temporary gauge, this discharge prior is used directly to calibrate a rating curve, and for BAM this discharge prior forms part of a likelihood function. In BAM, the output discharge estimate, or "posterior," is generated at the timestep of the water surface elevation data, providing a continuous discharge record. Table 2 describes which parameters we adapted in this study to fit to the TOWNS data set.

BAM uses truncated distributions for priors. We constrained Q_{prior} to the gauge distribution, limited Manning's n to physically realistic values at each cross section within the reach following Chow (1959) and a margin of error, and constrained A_0 to Manning's equation via inverting area based on observed width, slope, discharge, and our constraints on n. σ_Q, or the standard deviation of discharge, unlike the other standard deviations presented in Table 2, encompasses both the expected variability in discharge in time

and the error in the prior center, $\hat{Q}$. Together, $\hat{Q}$ and σ_Q make up the distribution of Q_{prior}. Additionally, we also constrained the range of upper and lower bounds for each parameter (*bounds*) using physically realistic values shown in Table 2, and based expected measurement errors in input data on the resolution of the input data. Constraining these parameters allowed us to test the sensitivity of the model based on these physical controls.

3.3. Temporary Gauge Comparison

For the temporary gauges, we used PT water levels and gauge discharge estimates to create rating curves. We treated each PT as its own temporary gauging station and developed a rating curve to estimate discharge over the validation deployment period, then summarized the ensemble of temporary gauges to compare to DAPT. In order to determine the sensitivity of a temporary gauge to the number of available discharges, we subsampled the available discharge and built separate rating curves for each subsample. To build the rating curve, we assumed a power-law relationship between WSE and discharge, as presented in Equation 2 where Q_t and H_t represent discharge and WSE at time t, and C_0, e, and B are coefficients:

$$Qt = Co * \left(Ht - e \right)^{B} \tag{2}$$

This method follows common field practice of relying on power-law rating curves to estimate discharge (Ashmore & Sauks, 2006; Dymond & Christian, 1982; Gleason & Smith, 2014; Herschy, 1993; Leon et al., 2006; Rantz, 1982; Smith et al., 1996; Smith & Pavelsky, 2008; World Meteorological Organization, 2010).

3.4. PAD Case Study

Similar to the TOWNS data set, we used BAM to estimate discharge within the PAD, but key differences were that we did not have gauge records for calibration and that available DEMs have lower resolution. In the TOWNS data set, validation discharge was derived from a permanent gauge rating curve. As a result, the relationship between our logged predictor (WSE) and logged output (discharge) is strong with a mean R^2 value of 0.79, while in the PAD the correlation is weaker, with a mean R^2 value of 0.25. These differences motivate the need to treat and validate TOWNS and PAD sites separately, and we proceed to describe these departures below. Although BAM relies on Manning's equation (i.e., not a rating curve) to estimate discharge, the input is still driven by observations of WSE.

To obtain input data in the PAD, we used the PT arrays described in Table 1 to calculate the change in river height, and we relied on a manually digitized centerline and a DEM to estimate distance along the river between transducers, shown in Figure 3. Unlike the TOWNS data, we held widths constant as determined at the time of installation using a rangefinder instead of relying on the CDEM, thus our widths do not vary with time. This departure from the TOWNS methodology was due to the deltaic landscape characterized by low gradients for which a coarse DEM is unable to delineate water-land separations and thus does not yield accurate river widths.

Instead of using a gauge to constrain priors in the PAD, we instead relied on ADCP measurements, and we also used the results from the TOWNS data set to better constrain priors by applying the optimal TOWNS parameters in Table 2 in cases where our PAD measurements cannot provide them a priori. However, without a gauge or high frequency ADCP measurements to provide Q_{prior}, our prior constraint estimates were suboptimal. In an attempt to overcome underestimating the sensitive σ_Q prior, we set this value to be greater than or equal to the average of normalized σ_Q for the TOWNS data set, as TOWNS sensitivity results indicate that larger σ_Q improves BAM estimation. In addition to estimating discharge for the validation time period (i.e., times when ADCP measurements were made) for DAPT, we also estimated discharge for the entire time period for which the PTs were installed, ranging from a few weeks to a few months depending on the river, as shown in Table 1. For this longer time period, we compared flow dynamics with nearby gauges that are not mass conserved with our reaches, but likely emulate similar patterns.
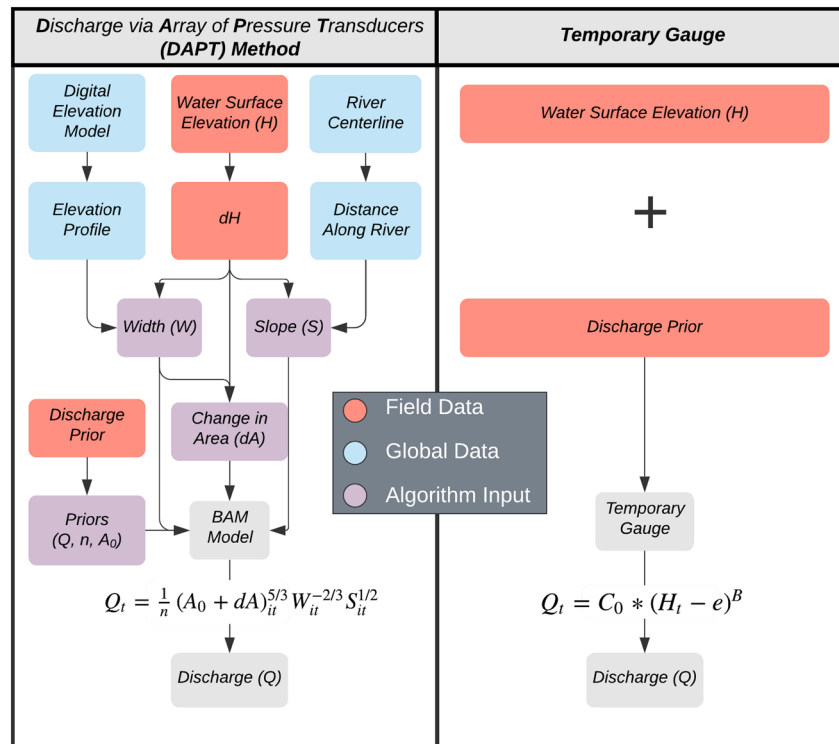
Figure 3. Depicted on the left for the DAPT method is the workflow to obtain BAM inputs (width, slope, and partial area) from data sources (WSE, DEM, and location of the river centerline). The change in height (*dH*) immediately follows from WSE and represents the change in elevation between river locations. BAM uses these inputs alongside prior estimates needed to solve Manning's equation (Equation 1) to estimate discharge. On the right, a temporary gauge relies on WSE measurements tied to discharge measurements to create a rating curve to estimate discharge (Equation 2). BAM, Bayesian-AMHG-Manning; DAPT, discharge via arrays of pressure transducers; DEM, digital elevation models; WSE, water surface elevation.

3.5. Validation

We relied on a combination of two error metrics to validate all hydrographs. Nash Sutcliffe Efficiency (NSE) compares model performance to the mean of observations and is optimal at a value of 1. Kling Gupta Efficiency (KGE) is a metric that combines correlation coefficient, bias ratio, and variability ratio and is also optimal at 1. These are both standard skill metrics widely used in hydrology.

4. Results

4.1. Q1: How Robust is DAPT to Changes in Input Data and Model Parameters?

In each TOWNS river, DAPT closely matches the observed daily discharge within a relatively narrow variability range as displayed by the small shaded interquartile region (IQR; Figure 4). In general, DAPT tends to capture mean flow, but there are some exceptions in the Olentangy and Willamette, where it underestimates peak flows within the interquartile range of the sensitivities. Under optimal parameter settings, DAPT captures flows at all ranges, with a mean NSE across all rivers of 0.92. When taking into account all 4,954 sensitivity tests, the average NSE across rivers falls to 0.79. Overall, these results confirm the ability of DAPT to closely replicate the discharge record across all tests in the TOWNS data set with the aid of a nearby gauge to optimize model parameters and discharge inputs.

Our TOWNS sensitivity analyses focused on the effect of PT resolution and model parameters to constrain BAM. As a reminder, these sensitivity tests modulate the parameters, inputs, and priors that control DAPT by varying them across ranges of plausible values. Differences across these tests are relatively small (Figure 5), highlighting the overall robustness of this method under these ideal conditions. As corroborated
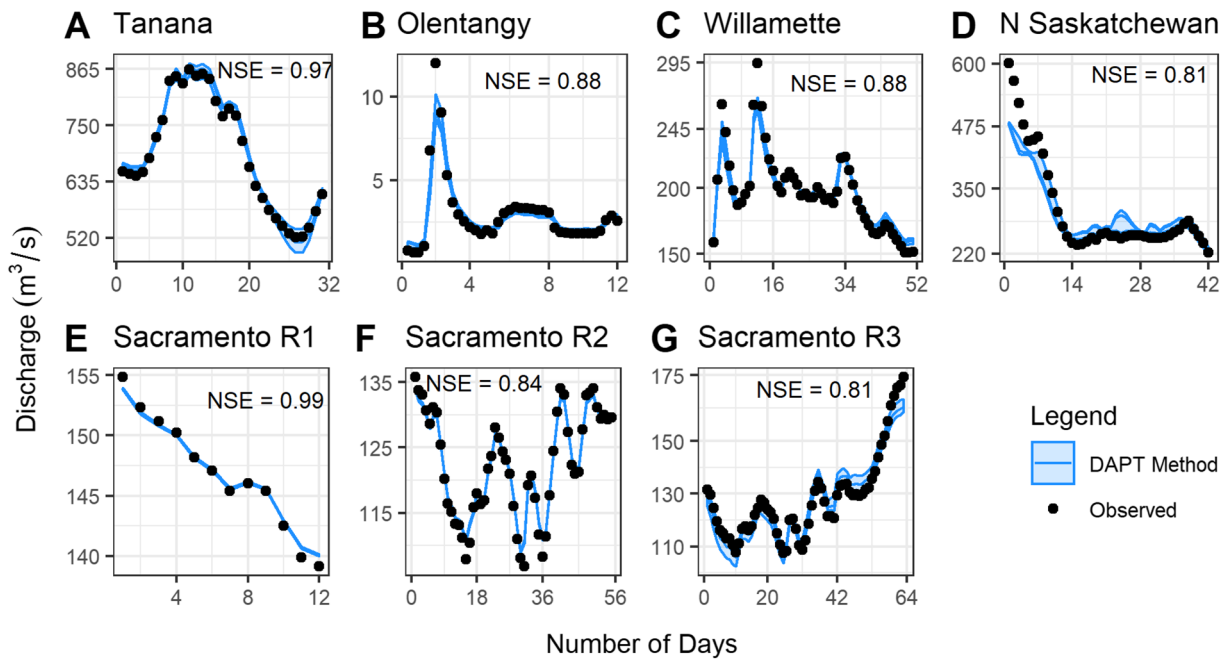
Figure 4. TOWNS hydrographs of all seven reaches. BAM is represented by the blue lines and shaded areas, whereas the gauge is shown in black circles. The solid line represents the median discharge across all 4,954 sensitivity tests over the given time period, and the shaded region represents the first and third quartile of all sensitivity tests described in Figure 1 (number of PTs, spacing of PTs, BAM parameters, and observed discharge). NSE values correspond to the best-performing test for each river. BAM, Bayesian-AMHG-Manning; NSE, Nash Sutcliffe Efficiency.

by the hydrographs in Figure 4, DAPT performance is on average quite skillful, with many of the violin plots concentrated near optimal values of 1 in Figure 5. The most sensitive parameter is the sample size of observed discharge measurements used to constitute the prior for discharge (numQ_{prior}), indicating that a larger sample size to estimate Q_{prior} is crucial to effectively reproduce discharge (Figure 5).

The relative insensitivity of the remaining parameters and PT resolutions is encouraging; if discharge is adequately constrained, a solid understanding of the remaining priors or a certain threshold of PT resolution is less important. For example, the difference between 2 and 20 PTs is insignificant compared to the difference between 2 and 20 discharge measurements included in Q_{prior}. This finding implies that with a good prior understanding of discharge, DAPT can reproduce discharge at high temporal resolution by relying on only a few PTs.

The results of changing PT spatial and temporal resolution (Figure 5, Panel A) are less sensitive than changes in BAM parameters and discharge (Panel B), particularly with regards to outliers, but noteworthy nevertheless in the implications for method design. The violin plots in Figure 5 are mirrored pdfs, such that the thicker the shaded area, the more common the value. The long tails of the plots thus correspond to infrequent values. A sensitive test would have a violin plot of uniform thickness extending over a wide range, whereas an insensitive plot would have a single "bulb" around a narrow range of values. We thus interrogate these plots by examining the width of the range of values over which the violin plots show the highest concentrations of values KGE and NSE show similar patterns with a higher concentration of sensitivity tests toward the optimal end, and longer, thinner tails toward the worse metrics, with NSE showing more favorable results. Aggregating to a daily timestep, altering the spacing between PTs, or decreasing the number of PTs all have negligible effects (Figure 5).

The number of samples in the discharge prior (numQ_{prior}), on the other hand, is sensitive, implying that subsampling just part of Q_{prior} can significantly degrade model performance. This implication is realized in Panels D–F in Figure 6, where mischaracterizing Q_{prior} or relying on only a few discharge samples substantially worsens results. We find that increasing the number of discharge estimates in Q_{prior} and increasing the variability of those estimates improves overall performance of DAPT. In cases with substantial "breaks" in observed WSE, it is important that Q_{prior} is sampled from each side of the break (e.g., the Olentangy).
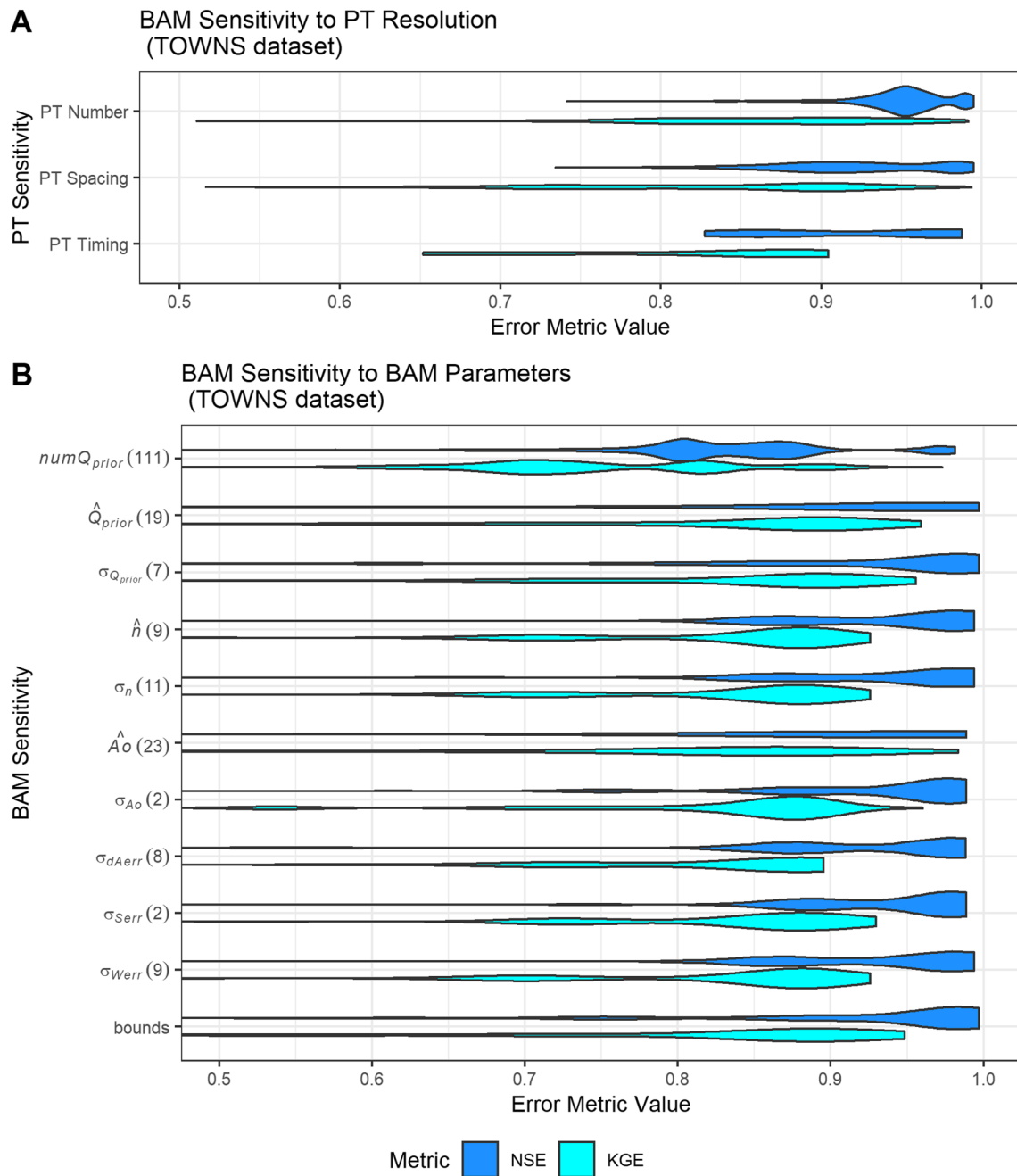
Figure 5. TOWNS sensitivity broken down by each sensitivity category (PT resolutions in Panel A and BAM parameters in Panel B). Each violin plot summarizes these tests across all rivers. Model performance is measured through Nash Sutcliffe Efficiency (NSE), and Kling Gupta Efficiency (KGE), both considered optimal at 1. Results are truncated at 0.5 for viewing purposes, and number of data points not shown are counted in the parentheses following each test. Results that are more sensitive have uniform distributions, while concentrated distributions are less sensitive: the "bulb" in the violin plot indicates a more common value. BAM, Bayesian-AMHG-Manning.

Interestingly, as the number of PTs increases, model performance slightly decreases, since more PTs incorporate more variance within channel geometry and the assumption of mass conservation becomes less stable. This may be slightly counterintuitive, as readers may expect more data to produce better results. However, these results indicate that these extra data confound the Bayesian likelihood rather than improve it.
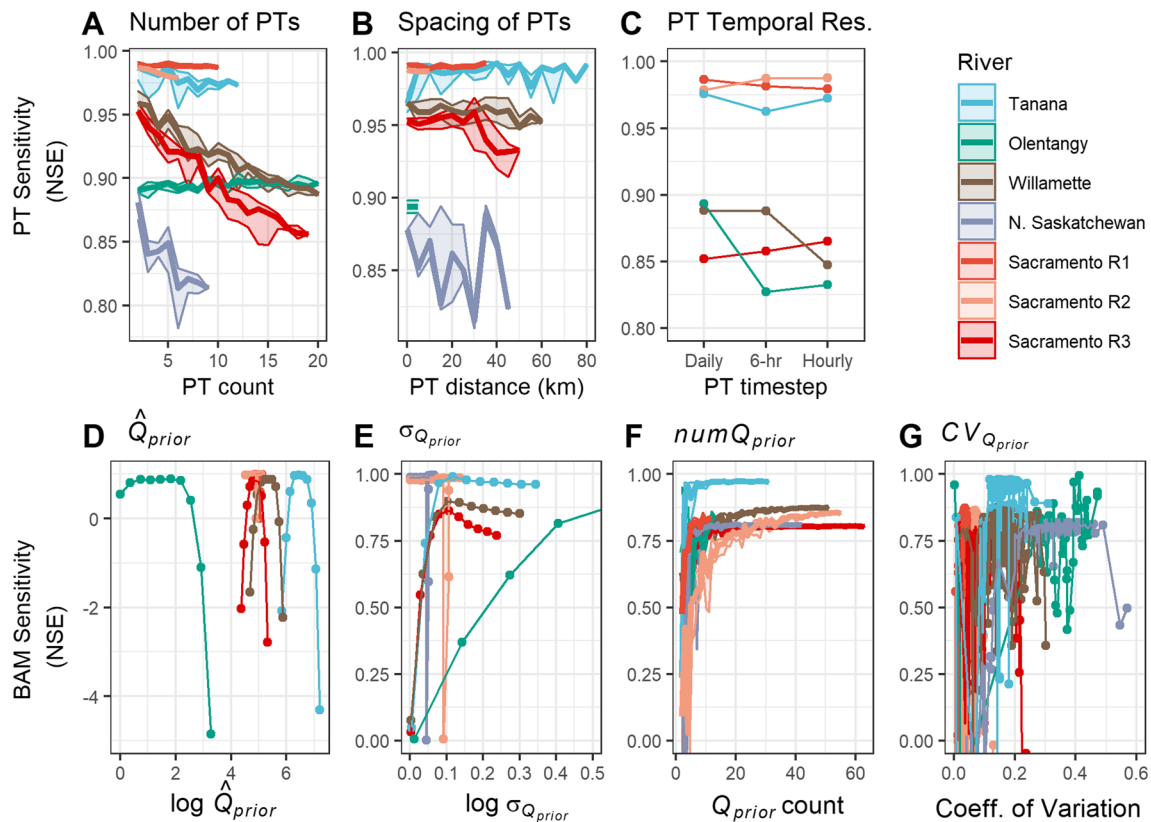
Figure 6. TOWNS sensitivities for the PT sensitivity (Panels A–C), and discharge parameters in BAM sensitivity (Panels D–G). The *x*-axis represents the value of each prior tested, and the *y*-axis is model performance measured by NSE, considered optimal at 1. PT resolution in general is relatively insensitive. Panel D shows that either over or underestimating discharge substantially degrades model performance, while Panel E (truncated), shows that underestimating discharge standard deviation has a negative effect. Panels F and G are truncated to highlight differences between rivers, and performance generally increases as the number of samples within the discharge count (Panel F) and variability (measured by coefficient of variation CV) of the discharge count increase (Panel G). BAM, Bayesian-AMHG-Manning; NSE, Nash Sutcliffe Efficiency.

4.2. Q2: How Does DAPT Compare to a Temporary Gauge?

To compare DAPT with a temporary gauge, we used the USGS gauge record as Q_{prior} for both DAPT and a temporary gauge. We then conducted a sensitivity analysis (Test 5; Figure 6 Panel F) to the number and variability of discharge estimates in this prior data set. To compare these results, we compare the error metrics for both methods over the validation period. Figure 7 Panel A shows 72% of DAPT estimates are within 0.10 NSE of a temporary gauge ensemble. Figure 7 Panels B–G combine the results of discharge sensitivity shown earlier in Figure 6. In the Tanana and Sacramento R3 both methods perform similarly, whereas in the Olentangy and Sacramento R2 DAPT outperforms a temporary gauge. In the Olentangy in particular, the temporary gauge performance is unstable largely arising from discharge samples that omit a single peak flow in the data record, with a median NSE of 0.87 including the peak flow and median NSE of −9.3 omitting the peak flow. In comparison, DAPT is relatively robust with identical medians of 0.77 for samples with and without the peak flow. Finally, in the Willamette, North Saskatchewan, and Sacramento R1, the temporary gauge outperforms DAPT.

4.3. Q3: How Well Can DAPT Reproduce In Situ Discharge Measurements in a Realistic Field Setting?

To address Q3, we validated DAPT with in situ ADCP-based discharge measurements in the PAD. Here we validated on two fronts: quantitatively across the validation period (the time period ADCP measurements were taken), and qualitatively across the entire PT deployment period for each reach using nearby permanent ECCC gauges for comparison. Over the validation time period, DAPT closely approximates the ADCP
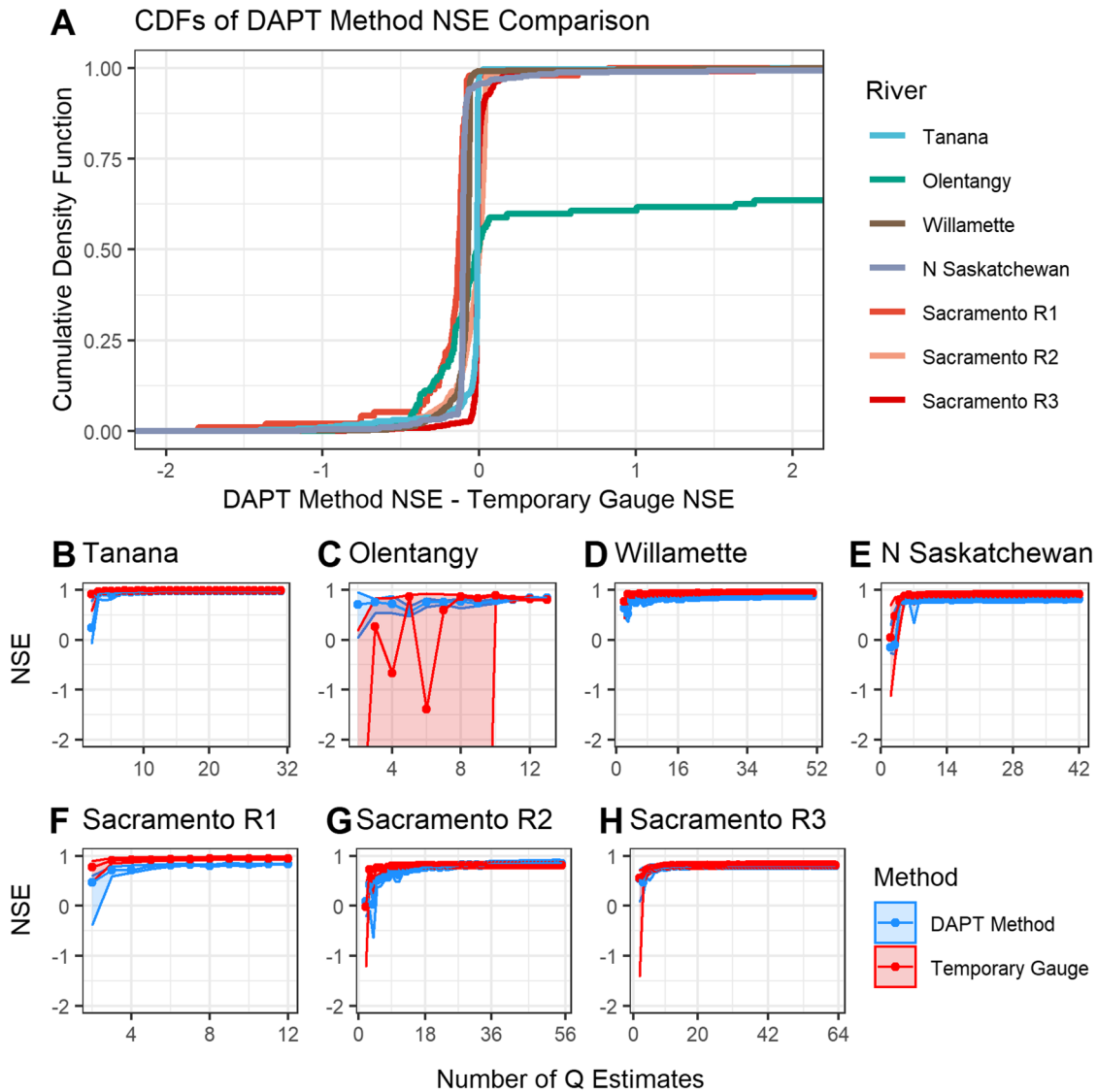
Figure 7. TOWNS comparison between DAPT and a temporary gauge. Panel A displays the difference for all rivers in NSE between the temporary gauge and DAPT in a cumulative density function, hence positive values show that DAPT outperforms the temporary gauge. 72% of the comparisons are between ± 0.1 NSE, indicating that DAPT and the temporary gauges are largely equivalent in this ideal setting. Panels B–H show NSE as a function of the number of discharge measurements for each river individually. DAPT, discharge via arrays of pressure transducers; NSE, Nash Sutcliffe Efficiency.

time series and is relatively robust to the number of ADCP measurements used to constrain this method, as the IQR across all samples of ADCP measurements closely matches the observed record (Figure 8). The temporary gauge, in comparison, is not adequately trained as the water levels remain relatively static over this time period (Figure 8). As such, the temporary gauge fails to capture either high or low flows. Since the power-law relationship between water surface elevation and discharge is not fully developed or appropriate in this case, more prior discharge data would be needed to improve the temporary gauge. Therefore, the DAPT method is better suited for and designed for this context: many rivers and limited field time and budget.

The validation time period during which ADCP measurements were made represents a short and misrepresentative span of the entire PT deployment period, as shown in Figure 9. Thus, we must also look at discharge estimation over the entire deployment time to further understand this comparison. Figure 9 shows hydrographs for each of the 11 reaches within the nine PAD rivers across the entire time period for which
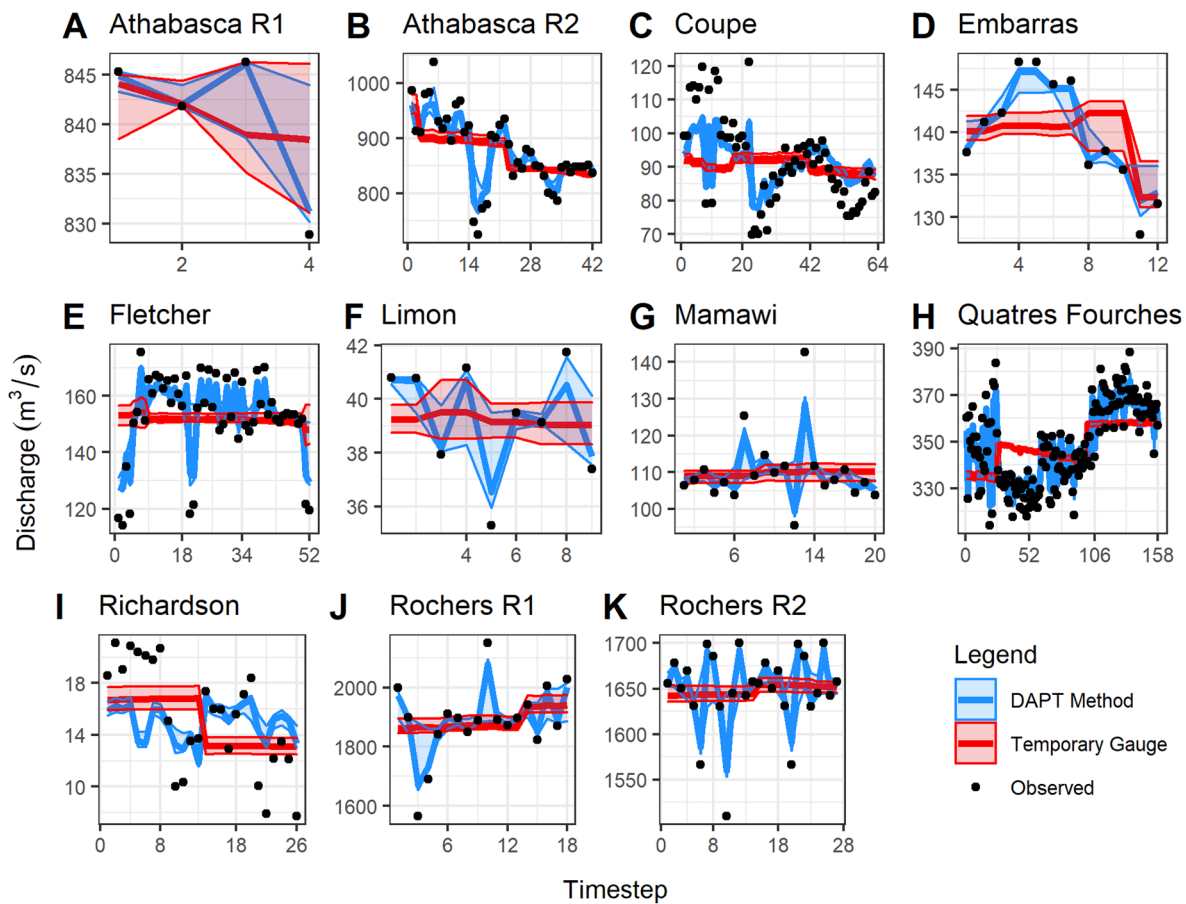
Figure 8. Hydrographs of the validation period. The *x*-axes represent the nth ADCP measurement, as the time between samples varies for each measurement and river. Blue lines represent the median hydrograph for the DAPT method, with shaded regions representing the IQR across the sensitivity to the number of ADCP measurements used to constrain each method. Temporary gauge estimates are displayed in red and are developed across a range of identical samples to the DAPT method from identical PT and ADCP data. ADCP, acoustic doppler current profiler; DAPT, discharge via arrays of pressure transducers; IQR, interquartile region.

the PTs were installed. As DAPT discharge bounds are constrained by ADCP measurements, DAPT tends to estimate discharge within the range of observed ADCP values throughout the entire time series producing relatively stagnant hydrographs, while nearby gauges show more dynamism over this period. DAPT dynamics do track nearby gauges, but this qualitative assessment can only state as much.

5. Discussion

In essence, we have taken a method designed to retrieve discharge from global satellite data and reimagined it for in situ field campaigns. Our results indicate that DAPT is a viable discharge estimation option, as it closely replicates gauge discharge under optimal conditions (Figure 4) and performs adequately in remote settings. As expected, overall performance was closely tied to the ability to correctly calculate BAM model parameters, notably Q_{prior}. In the TOWNS case where gauges were used to constrain BAM, all rivers, including very large, braided rivers such as the Tanana as well as leveed rivers such as the three Sacramento reaches displayed robust results, and these results were relatively insensitive to changes in PT resolution. This signifies the universality of this method, and implies that when well calibrated, DAPT can reproduce discharge in a variety of field settings.

In our comparison with a temporary gauge in TOWNS, we found that both methods perform similarly. However, we note that this comparison favors a temporary gauge from the outset, as the gauge record is derived from a rating curve and presents a best-case scenario for a temporary gauge. In a true field setting,
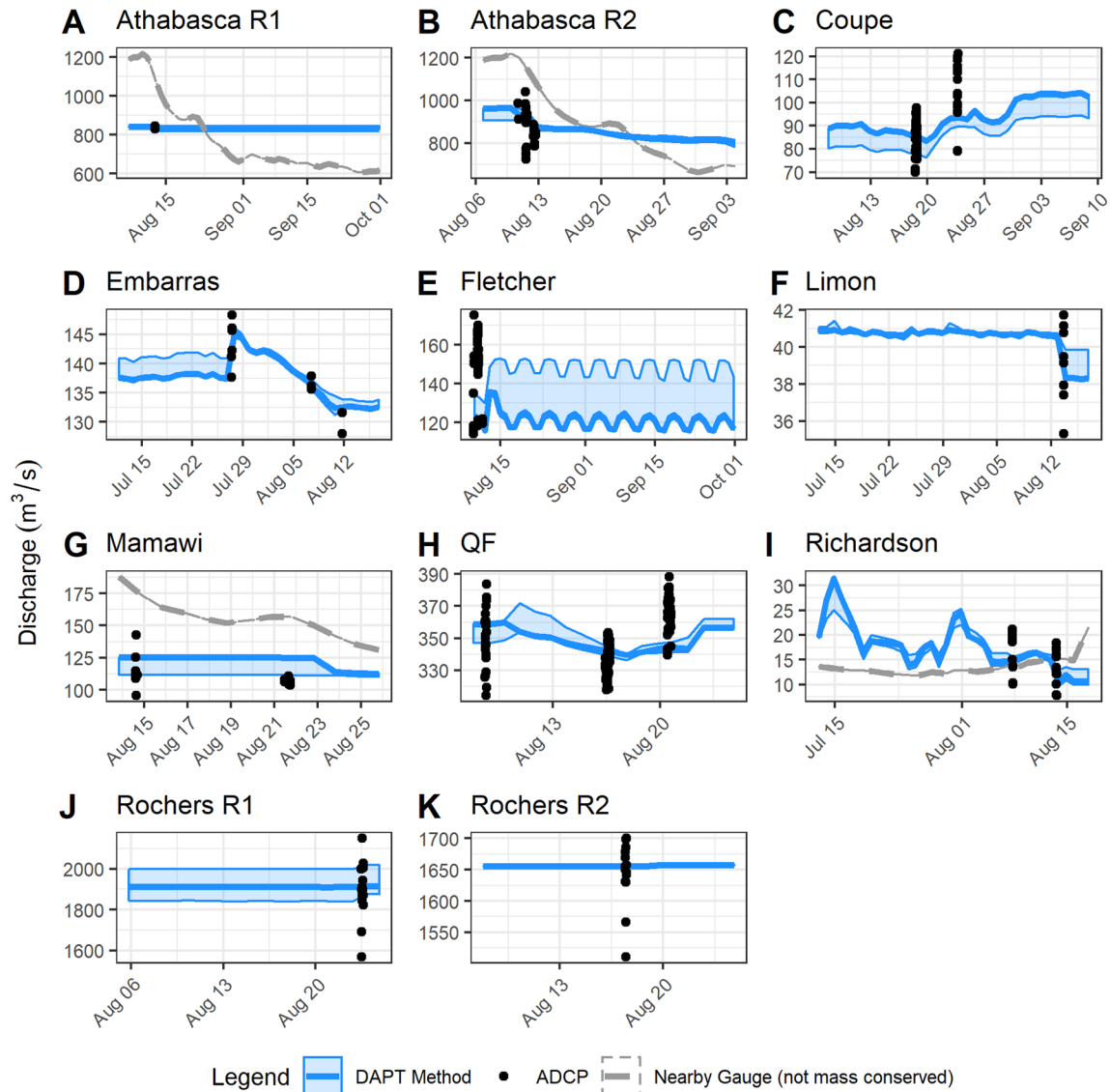
Figure 9. PAD 2018 and 2019 hydrographs for each of the nine rivers and 11 reaches over the entire time period of PT deployment. The DAPT method is shown in blue with a solid line representing the median hydrograph across the sensitivity to the number of ADCP measurements (black) used, with the IQR shown shaded. Note that the nearby gauges (gray, dashed) are not mass conserved and highlight only temporal trends, not accuracy of the methods, and serve as qualitative validation. ADCP, acoustic doppler current profiler; DAPT, discharge via arrays of pressure transducers; IQR, interquartile region; PAD, Peace-Athabasca Delta.

in situ discharge measurements may present weaker relationships with stage or contain additional errors or uncertainty, such as those seen in the PAD ADCP data. When only a few measurements are included with low sample variance, the DAPT method tends to perform better than a temporary gauge, and DAPT is less dependent on the quality of discharge priors. The robustness of DAPT implies that this method could estimate discharge with fewer in situ measurements over a less dynamic range. Therefore, if time and budget only allow only a few ADCP measurements, then DAPT could be applied to several rivers over a wide area in a shorter time than would be needed to fully develop rating curves. Thus, we feel this method could be a good alternative or supplement to the traditional approach of installing a temporary gauge when developing a rating curve is infeasible, especially in remote sites.

Our PAD case study represents one of these sites, where developing a full rating curve at each river was impractical for the magnitude of rivers covered in a month(s) long period. In the PAD, the DAPT method is able to accurately reproduce an ADCP discharge record, particularly for when a high number of ADCP

measurements were used. Although this "perfect" discharge case in and of itself might seem trivial in that the output is simply reproducing the input data, we note the temporary gauge could not match this performance (Figure 8). This highlights an additional strength of DAPT in that it is not tightly bound to a singular mathematical relationship (i.e., the power law in a gauge) but has additional flexibility that allows it to replicate discharge where traditional flow laws and rating curves cannot (Table 1, Figure 8). This performance in the PAD has one exception in the Richardson, where the DAPT method fails to fully capture the observed record, potentially due to the size of the river, which compromised the quality of the ADCP data as the boat was not able to complete a full transect at low enough speed, and compromised prior assumptions within BAM, which was not trained on small rivers.

Comparing time and effort, the DAPT method can be employed in a substantially shorter time than a temporary gauge, allowing more rivers to be monitored in a field season. We argue it would not have been possible to build a quality temporary gauge in all 11 reaches in the two summer-only field seasons we visited the PAD, and that DAPT was the most viable and accurate path toward improved hydrologic understanding of the PAD. Because the PAD case study was specifically designed to mimic a realistic remote field setting for which a temporary gauge may not be suitable to begin with, obtaining a longer ADCP record would have either resulted in a substantially longer field campaign or only focusing on one river instead of 11 reaches. Indeed, adequate data collection for a temporary gauge was never achieved in this case study across our 11 reaches.

To better parse the difference between a temporary gauge and DAPT, future studies could rely on a more thorough ADCP time series to build more comparable temporary gauges, which would further delineate challenges observed in these two datasets, such as those related to the gauge records, ADCPs, temporal discharge resolution, and PAD-specific limitations. However, obtaining such a record would obviate the need for the DAPT method as a temporary gauge would fit the data well at that point. Further, this substantial effort would likely only re-verify the TOWNS results presented here. Our case study (two summer field campaigns to a remote sub-Arctic delta) represents conditions frequently experienced by hydrologists and is a realistic marker of perhaps the best way to collect a temporary discharge record over a large area in a short time.

Another path forward includes a further look into the ability of DAPT to estimate discharge without any ADCP measurements or a gauge. We did not explicitly explore the case where a global model is used as Q_{prior}, which would eliminate the need for an ADCP or gauge altogether. The PAD is poorly represented in globally available hydrology models, as its complex deltaic channels and occasionally reversing flow direction require a hydraulic sophistication (see Peters et al., 2006; Pietroniro et al., 2000) not typically available from "off the shelf" model output. We are confident that DAPT would work well for the PAD in the absence of any ADCP work if a model could give an accurate estimate of Q_{prior} (following the TOWNS results and Hagemann et al., 2017), but in this case ADCP measurements were needed for both DAPT and the temporary gauge.

Other areas of improvement include exploring higher resolution DEMs, such as UAV-based or Lidar DEMs, which would allow for more accurate and contemporaneous width and slope extraction. Higher-resolution DEMs would also allow for better width extraction methods, including nonlinear interpolation following Mersel et al. (2013) and Schaperow et al. (2019). If high-resolution bathymetry were obtained (e.g., through a UAV, or aerial imagery during low-flow conditions, or ADCP bathymetry), then following King et al. (2018) it would be possible to pair PTs with hydraulic modeling to estimate discharge. Additionally, incorporating ADCP bathymetry into the parameters would allow for more accurate width and area estimates that vary temporally, and would likely improve AMHG estimates, which rely on variations in width alone.

Looking toward the overall utility of this method, both the TOWNS tests and PAD case study indicate that estimating discharge with the DAPT method can be a precise and efficient means of field discharge estimation. Even in the PAD where parameters were sub-optimally fit, DAPT definitively replicated an ADCP for the validation period while highlighting its main strengths: accurate in situ discharge estimation with little to no discharge measurements in a region or time frame that is not conducive to relying on or installing a temporary or permanent gauge.

6. Conclusion

We introduced a novel in situ method to estimate discharge in poorly gauged basins using arrays of pressure transducers (DAPT). Through five sensitivity tests, we validated and assessed the robustness of DAPT in five gauged rivers and in a realistic field setting. We found that DAPT performs similarly to a temporary gauge and can reproduce ADCP discharge data in a complex boreal river delta over two years of dedicated field experiments, given a threshold of at least 3–5 initial discharge estimates. We recommend the DAPT method for rivers or studies in which obtaining a long-term ADCP record or installing a gauge is infeasible, as the method is relatively robust to imperfect discharge priors. We note that this non-traditional method for small field rivers was spurred by developments in global remote sensing and hydrology via the SWOT satellite mission and suggest that future work that translates remote sensing paradigms for field study may be fruitful.

Data Availability Statement

Upon acceptance, Water surface elevation data, ADCP data and code to run the model and reproduce our figures can be found at http://doi.org/10.5281/zenodo.4569176. All other data required to reproduce this study are freely available online. Digital elevation models can be downloaded at (https://www.usgs.gov/core-science-systems/ngp/tnm-delivery/) for the contiguous United States, (https://www.pgc.umn.edu/data/arcticdem/) within the Arctic, and (https://open.canada.ca/data/en/dataset/7f245e4d-76c2-4caa-951a-45d1d2051333) within Canada. Discharge data can be downloaded at USGS for the United States (https://waterdata.usgs.gov/nwis) and here for Canada: (https://wateroffice.ec.gc.ca/).

References

Allen, G. H., & Pavelsky, T. M. (2018). Global extent of rivers and streams. *Science*, *361*(6402), 585–588. https://doi.org/10.1126/science.aat0636

Alsdorf, D. E., Rodríguez, E., & Lettenmaier, D. P. (2007). Measuring surface water from space. *Reviews of Geophysics*, *45*(2). https://doi.org/10.1029/2006RG000197

Altenau, E. H., Pavelsky, T. M., Bates, P. D., & Neal, J. C. (2017a). The effects of spatial resolution and dimensionality on modelling regional-scale hydraulics in a multichannel river. *Water Resources Research*, *53*(2), 1683–1701. https://doi.org/10.1002/2016WR019396

Altenau, E. H., Pavelsky, T. M., Moller, D., Lion, C., Pitcher, L. H., Allen, G. H., et al. (2017b). AirSWOT measurements of river water surface elevation and slope: Tanana River, AK. *Geophysical Research Letters*, *44*(1), 181–189. https://doi.org/10.1002/2016GL071577

Andreadis, K. M., Brinkerhoff, C. B., & Gleason, C. J. (2020). Constraining the assimilation of SWOT observations with hydraulic geometry relations. *Water Resources Research*, *56*(5), e2019WR026611. https://doi.org/10.1029/2019WR026611

Ashmore, P., & Sauks, E. (2006). Prediction of discharge from water surface width in a braided river with implications for at-a-station hydraulic geometry. *Water Resources Research*, *42*(3). https://doi.org/10.1029/2005WR003993

Biancamaria, S., Lettenmaier, D. P., & Pavelsky, T. M. (2016). The SWOT mission and its capabilities for land hydrology. *Surveys in Geophysics*, *37*(2), 307–337. https://doi.org/10.1007/s10712-015-9346-y

Birkinshaw, S. J., Moore, P., Kilsby, C. G., O'Donnell, G. M., Hardy, A. J., & Berry, P. A. M. (2014). Daily discharge estimation at ungauged river sites using remote sensing. *Hydrological Processes*, *28*(3), 1043–1054. https://doi.org/10.1002/hyp.9647

Bjerklie, D. M., Birkett, C. M., Jones, J. W., Carabajal, C., Rover, J. A., Fulton, J. W., & Garambois, P.-A. (2018). Satellite remote sensing estimation of river discharge: Application to the Yukon River Alaska. *Journal of Hydrology*, *561*, 1000–1018. https://doi.org/10.1016/j.jhydrol.2018.04.005

Bjerklie, D. M., Dingman, S. L., Vorosmarty, C. J., Bolster, C. H., & Congalton, R. G. (2003). Evaluating the potential for measuring river discharge from space. *Journal of Hydrology*, *278*(1), 17–38. https://doi.org/10.1016/S0022-1694(03)00129-X

Bjerklie, D. M., Moller, D., Smith, L. C., & Dingman, S. L. (2005). Estimating discharge in rivers using remotely sensed hydraulic information. *Journal of Hydrology*, *309*, 191–209. https://doi.org/10.1016/j.jhydrol.2004.11.022

Brakenridge, G. R., Cohen, S., Kettner, A. J., Groeve, T. D., Nghiem, S. V., Syvitski, J. P. M., & Fekete, B. M. (2012). Calibration of satellite measurements of river discharge using a global hydrology model. *Journal of Hydrology*, *475*, 123–136. https://doi.org/10.1016/j.jhydrol.2012.09.035

Brakenridge, G. R., Nghiem, S. V., Anderson, E., & Mic, R. (2007). Orbital microwave measurement of river discharge and ice status. *Water Resources Research*, *43*(4). https://doi.org/10.1029/2006WR005238

Canova, M. G., Fulton, J. W., & Bjerklie, D. M. (2016). *USGS HYDRoacoustic dataset in support of the Surface Water Oceanographic Topography satellite mission (HYDRoSWOT) [Data set]*. U.S. Geological Survey. https://doi.org/10.5066/F7D798H6

Chaudhury, R. R., Sobrinho, J. A. H., Wright, R. M., & Sreenivas, M. (1998). Dissolved oxygen modeling of the Blackstone River (northeastern United States). *Water Research*, *32*(8), 2400–2412. https://doi.org/10.1016/S0043-1354(98)00004-9

Chow, V. T. (1959). *Open-channel hydraulics*. New York, NY: McGraw-Hill.

Coxon, G., Freer, J., Westerberg, I. K., Wagener, T., Woods, R., & Smith, P. J. (2015). A novel framework for discharge uncertainty quantification applied to 500 UK gauging stations. *Water Resources Research*, *51*(7), 5531–5546. https://doi.org/10.1002/2014WR016532

Dingman, S. L., & Bjerklie, D. M. (2006). Estimation of river discharge. In *Encyclopedia of hydrological sciences*. American Cancer Society. https://doi.org/10.1002/0470848944.hsa069

Durand, M. T., Neal, J., Rodriguez, E., Andreadis, K. M., Smith, L. C., & Yoon, Y. (2014). Estimating reach-averaged discharge for the River Severn from measurements of river water surface elevation and slope. *Journal of Hydrology*, *511*, 92–104. https://doi.org/10.1016/j.jhydrol.2013.12.050

Durand, M. T., Rodriguez, E., Alsdorf, D. E., & Trigg, M. (2010). Estimating river depth from remote sensing swath interferometry measurements of river height, slope, and width. *IEEE Journal of Selected Topics in Applied Earth Observations and Remote Sensing*, *3*, 20–31. https://doi.org/10.1109/JSTARS.2009.2033453

Dymond, J. R., & Christian, R. (1982). Accuracy of discharge determined from a rating curve. *Hydrological Sciences Journal*, *27*(4), 493–504. https://doi.org/10.1080/02626668209491128

Fekete, B. M., Looser, U., Pietroniro, A., & Robarts, R. D. (2012). Rationale for monitoring discharge on the ground. *Journal of Hydrometeorology*, *13*(6), 1977–1986. https://doi.org/10.1175/JHM-D-11-0126.1

Feng, D., Gleason, C. J., Yang, X., & Pavelsky, T. M. (2019). Comparing discharge estimates made via the BAM algorithm in high-order Arctic rivers derived solely from optical CubeSat, Landsat, and Sentinel-2 data. *Water Resources Research*, *55*(9), 7753–7771. https://doi.org/10.1029/2019WR025599

Garambois, P.-A., & Monnier, J. (2015). Inference of effective river properties from remotely sensed observations of water surface. *Advances in Water Resources*, *79*, 103–120. https://doi.org/10.1016/j.advwatres.2015.02.007

Gleason, C. J., & Durand, M. T. (2020). Remote sensing of river discharge: A review and a framing for the discipline. *Remote Sensing*, *12*(7), 1107. https://doi.org/10.3390/rs12071107

Gleason, C. J., Garambois, P.-A., & Durand, M. T. (2017). Tracking river flows from space. *Eos*, *98*. https://doi.org/10.1029/2017EO078085

Gleason, C. J., & Hamdan, A. (2015). Crossing the (watershed) divide: Satellite data and the changing politics of international river basins. *The Geographical Journal*, *183*. https://doi.org/10.1111/geoj.12155

Gleason, C. J., & Smith, L. C. (2014). Toward global mapping of river discharge using satellite images and at-many-stations hydraulic geometry. Proceedings of the National Academy of Sciences of the United States of America, 111. https://doi.org/10.1073/pnas.1317606111

Hagemann, M. W., Gleason, C. J., & Durand, M. T. (2017). BAM: Bayesian AMHG-manning inference of discharge using remotely sensed stream width, slope, and height. *Water Resources Research*, *53*. https://doi.org/10.1002/2017WR021626

Hannah, D., Demuth, S., Van Lanen, H., Looser, U., Prudhomme, C., Rees, G., et al. (2011). Large-scale river flow archives: Importance, current status and future needs. *Hydrological Processes*, *25*, 1191–1200. https://doi.org/10.1002/hyp.7794

Herbert, L. R., & Thomas, B. K. (1992). *Seepage study of the Bear River including cutler reservoir in Cache Valley, Utah and Idaho*. Utah Department of Natural Resources, Division of Water Rights.

Herschy, R. (1993). The velocity-area method. *Flow Measurement and Instrumentation*, *4*(1), 7–10. https://doi.org/10.1016/0955-5986(93)90004-3

Horner, I., Renard, B., Le Coz, J., Branger, F., McMillan, H. K., & Pierrefeu, G. (2018). Impact of stage measurement errors on streamflow uncertainty. *Water Resources Research*, *54*(3), 1952–1976. https://doi.org/10.1002/2017WR022039

Huang, Q., Long, D., Du, M., Han, Z., & Han, P. (2020). Daily continuous river discharge estimation for ungauged basins using a hydrologic model calibrated by satellite altimetry: Implications for the SWOT mission. *Water Resources Research*, *56*(7), e2020WR027309. https://doi.org/10.1029/2020WR027309

Huang, Q., Long, D., Du, M., Zeng, C., Qiao, G., Li, X., et al. (2018). Discharge estimation in high-mountain regions with improved methods using multisource remote sensing: A case study of the Upper Brahmaputra River. *Remote Sensing of Environment*, *219*, 115–134. https://doi.org/10.1016/j.rse.2018.10.008

Kiang, J. E., Gazoorian, C., McMillan, H., Coxon, G., Coz, J. L., Westerberg, I. K., et al. (2018). A Comparison of methods for streamflow uncertainty estimation. *Water Resources Research*, *54*(10), 7149–7176. https://doi.org/10.1029/2018WR022708

King, T. V., Neilson, B. T., & Rasmussen, M. T. (2018). Estimating discharge in low-order rivers with high-resolution aerial imagery. *Water Resources Research*, *54*. https://doi.org/10.1002/2017wr021868

Kouraev, A., Zakharova, E., Samain, O., Mognard, N., & Cazenave, A. (2004). Ob' river discharge from TOPEX/Poseidon satellite altimetry (1992–2002). *Remote Sensing of Environment*, *93*, 238–245. https://doi.org/10.1016/j.rse.2004.07.007

Laenen, A., & Hansen, R. P. (1985). *Preliminary study of the water-temperature regime of the North Santiam River downstream from Detroit and big Cliff dams, Oregon (Water-Resources investigations report No. 84-4105)*. U.S. Geological Survey. https://doi.org/10.3133/wri844105

Leon, J. G., Calmant, S., Seyler, F., Bonnet, M.-P., Cauhopé, M., Frappart, F., et al. (2006). Rating curves and estimation of average water depth at the upper Negro River based on satellite altimeter data and modeled discharges. *Journal of Hydrology*, *328*(3), 481–496. https://doi.org/10.1016/j.jhydrol.2005.12.006

Mersel, M. K., Smith, L. C., Andreadis, K. M., & Durand, M. T. (2013). Estimation of river depth from remotely sensed hydraulic relationships. *Water Resources Research*, *49*(6), 3165–3179. https://doi.org/10.1002/wrcr.20176

Miller, E. G. (1962). *Observations of tidal flow in the Delaware River* (Vol. 33). U.S. Goverment Printing Office.

Minear, J. T., & Wright, S. A. (2016). *Water-surface elevations, depths, velocities, and temperature data collected for the NASA/JPL AirSWOT campaign on the Sacramento River, near Colusa, CA, for the period March–May, 2015*. U.SS Geological Survey Data Release. https://doi.org/10.5066/F7NZ85R4

Nathanson, M., Kean, J., Grabs, T., Seibert, J., Laudon, H., & Lyon, S. (2012). Modelling rating curves using remotely sensed LiDAR data. *Hydrological Processes*, *26*, 1427–1434. https://doi.org/10.1002/hyp.9225

Neal, J., Schumann, G., Bates, P., Buytaert, W., Matgen, P., & Pappenberger, F. (2009). A data assimilation approach to discharge estimation from space. *Hydrological Processes*, *23*(25), 3641–3649. https://doi.org/10.1002/hyp.7518

Oubanas, H., Gejadze, I., Malaterre, P.-O., Durand, M., Wei, R., Frasson, R. P. M., & Domeneghetti, A. (2018). Discharge estimation in ungauged basins through variational data assimilation: The potential of the SWOT mission. *Water Resources Research*, *54*(3), 2405–2423. https://doi.org/10.1002/2017WR021735

Paris, A., Paiva, R. D. D., Silva, J. S. D., Moreira, D. M., Calmant, S., Garambois, P.-A., et al. (2016). Stage-discharge rating curves based on satellite altimetry and modeled discharge in the Amazon basin. *Water Resources Research*, *52*(5), 3787–3814. https://doi.org/10.1002/2014WR016618

Pavelsky, T. M. (2014). Using width-based rating curves from spatially discontinuous satellite imagery to monitor river discharge. *Hydrological Processes*, *28*(6), 3035–3040. https://doi.org/10.1002/hyp.10157

Pavelsky, T. M., Durand, M. T., Andreadis, K. M., Beighley, R. E., Paiva, R. C. D., Allen, G. H., & Miller, Z. F. (2014). Assessing the potential global extent of SWOT river discharge observations. *Journal of Hydrology*, *519*, 1516–1525. https://doi.org/10.1016/j.jhydrol.2014.08.044

Perry, C. A. (2012). *Determination of streamflow of the Arkansas River near Bentley in South-central Kansas (scientific investigations report No. 2012-5059)*. U.S. Department of the Interior, U.S. Geological Survey.

Peters, D. L., Prowse, T. D., Pietroniro, A., & Leconte, R. (2006). Flood hydrology of the Peace-Athabasca Delta, northern Canada. *Hydrological Processes*, *20*(19), 4073–4096. https://doi.org/10.1002/hyp.6420

Pietroniro, A., Leconte, R., Peters, D. L., Prowse, T. D. (2000). *Application of a hydrodynamic model in a freshwater delta using remote sensing*. In International symposium on remote sensing and hydrology (Santa Fe, NM, USA, Apr. 2-7, 2000). IAHS-AISH Publication (Vol. 267, pp. 519–525). Wallingford: International Association of Hydrological Sciences.

Porter, C., Morin, P., Howat, I., Noh, M.-J., Bates, B., Peterman, K., et al. (2018). *ArcticDEM*, Harvard Dataverse, V1, Feb 2019. https://doi.org/10.7910/DVN/OHHUKH

Prowse, T., & Conly, F. M. (2000). Multiple-hydrologic stressors of a northern delta ecosystem. *Journal of Aquatic Ecosystem Stress and Recovery*, *8*, 17–26. https://doi.org/10.1023/A:1011483504849

Rantz, S. E. (1982). Measurement and computation of streamflow (USGS Numbered Series No. 2175). In Measurement and Computation of Streamflow (Vol. 2175). U.S. G.P.O. https://doi.org/10.3133/wsp2175

Sandberg, G. W., & Smith, C. J. (1995). *Seepage Study of the Sevier Rivier Basin above Sevier Bridge Reservoir, Utah 1988* (Vol. 59). U.S. Geological Survey.

Schaperow, J., Li, D., Margulis, S., & Lettenmaier, D. (2019). A curve-fitting method for estimating bathymetry from water surface height and width. *Water Resources Research*, *55*, 4288–4303. https://doi.org/10.1029/2019WR024938

Shope, C. L., Bartsch, S., Kim, K., Kim, B., Tenhunen, J., Peiffer, S., et al. (2013). A weighted, multi-method approach for accurate basin-wide streamflow estimation in an ungauged watershed. *Journal of Hydrology*, *494*, 72–82. https://doi.org/10.1016/j.jhydrol.2013.04.035

Sichangi, A. W., Wang, L., & Hu, Z. (2018). Estimation of river discharge solely from remote-sensing derived data: An initial study over the Yangtze River. *Remote Sensing*, *10*(9). https://doi.org/10.3390/rs10091385

Smith, L. C. (1997). Satellite remote sensing of river inundation area, stage, and discharge: A review. *Hydrological Processes*, *11*(10), 1427–1439. https://doi.org/10.1002/(SICI)1099-1085(199708)11:10<1427::AID-HYP473>3.0.CO;2-S

Smith, L. C., Isacks, B. L., Bloom, A. L., & Murray, A. B. (1996). Estimation of discharge from three braided rivers using synthetic aperture radar satellite imagery: Potential application to ungaged Basins. *Water Resources Research*, *32*(7), 2021–2034. https://doi.org/10.1029/96WR00752

Smith, L. C., & Pavelsky, T. M. (2008). Estimation of river discharge, propagation speed, and hydraulic geometry from space: Lena River, Siberia. *Water Resource Research*, *44*, W03427. https://doi.org/10.1029/2007WR006133

Sörengård, M., & Baldassarre, G. D. (2017). Simple vs complex rating curves: Accounting for measurement uncertainty, slope ratio and sample size. *Hydrological Sciences Journal*, *62*(13), 2072–2082. https://doi.org/10.1080/02626667.2017.1367397

Sun, W., Fan, J., Wang, G., Ishidaira, H., Bastola, S., Yu, J., et al. (2018). Calibrating a hydrological model in a regional river of the Qinghai–Tibet plateau using river water width determined from high spatial resolution satellite images. *Remote Sensing of Environment*, *214*, 100–114. https://doi.org/10.1016/j.rse.2018.05.020

Tarpanelli, A., Brocca, L., Barbetta, S., Faruolo, M., Lacava, T., & Moramarco, T. (2015). Coupling MODIS and radar altimetry data for discharge estimation in poorly gauged river basins. *IEEE Journal of Selected Topics in Applied Earth Observations and Remote Sensing*, *8*(1), 141–148. https://doi.org/10.1109/JSTARS.2014.2320582

Toth, B., Pietroniro, A., Conly, F. M., & Kouwen, N. (2006). Modelling climate change impacts in the Peace and Athabasca catchment and delta: I—Hydrological model application. *Hydrological Processes*, *20*(19), 4197–4214. https://doi.org/10.1002/hyp.6426

Tuozzolo, S., Langhorst, T., de Moraes Frasson, R. P., Pavelsky, T., Durand, M., & Schobelock, J. J. (2019a). The impact of reach averaging Manning's equation for an in-situ dataset of water surface elevation, width, and slope. *Journal of Hydrology*, *578*, 123866. https://doi.org/10.1016/j.jhydrol.2019.06.038

Tuozzolo, S., Lind, G., Overstreet, B., Mangano, J., Fonstad, M., Hagemann, M., et al. (2019b). Estimating river discharge with swath altimetry: A proof of concept using AirSWOT observations. *Geophysical Research Letters*, *46*(3), 1459–1466. https://doi.org/10.1029/2018GL080771

Turnipseed, D. P., & Sauer, V. B. (2010). Discharge measurements at gaging stations. In *Encyclopedia of hydrological sciences* (pp. 87).

Van Dijk, A. I. J. M. V., Brakenridge, G. R., Kettner, A. J., Beck, H. E., Groeve, T. D., & Schellekens, J. (2016). River gauging at global scale using optical and passive microwave remote sensing. *Water Resources Research*, *52*(8), 6404–6418. https://doi.org/10.1002/2015WR018545

Wiele, S. M., & Torizzo, M. (2003). *A stage-normalized function for the synthesis of stage-discharge relations for the Colorado River in Grand Canyon, Arizona (Water-Resources Investigations Report No. 03-4037)*. Tucson. U.S. Geological Survey. https://doi.org/10.3133/wri20034037

World Meteorological Organization. (2010). *Manual on stream gauging*. Geneva. World Meteorological Organization.

Yamazaki, D., Ikeshima, D., Sosa, J., Bates, P. D., Allen, G. H., & Pavelsky, T. M. (2019). MERIT hydro: A high-resolution global hydrography map based on latest topography dataset. *Water Resources Research*, *55*(6), 5053–5073. https://doi.org/10.1029/2019WR024873

Yoon, Y., Durand, M., Merry, C. J., Clark, E. A., Andreadis, K. M., & Alsdorf, D. E. (2012). Estimating river bathymetry from data assimilation of synthetic SWOT measurements. *Journal of Hydrology*, *464*(465), 363–375. https://doi.org/10.1016/j.jhydrol.2012.07.028

Ziegeweid, J. R., Silliker, R. J., & Densmore, B. K. (2015). *Revising water-surface elevation data for gages in Rainy Lake, Namakan reservoir, and selected eivers in Minnesota, United States and Ontario, Canada (Report to the International Joint commission No. 1042–400750)* (p. 45).